



Calcareous nannofossil biostratigraphy and paleoenvironmental variations across the upper Paleocene–lowermost Eocene at Gebel Nezzazat, West Central Sinai, Egypt

Atef M. Kasem¹ · Mahmoud M. Faris² · Osman M. Osman¹ · Ahmed Yehia E. Badawy¹ · Fatma Shaker³

Received: 9 June 2021 / Accepted: 2 January 2022 / Published online: 4 April 2022
© The Author(s) 2022

Abstract

Detailed lithostratigraphic and calcareous nannofossil biostratigraphic studies were carried out across the Paleocene–Eocene (P–E) that outcrops at Gebel Nezzazat (G. Nezzazat) in West Central Sinai (Egypt). The study interval spans from the upper part of the Tarawan Formation to the lowermost Thebes Formation covering the whole Esna Formation in between them. The Esna Formation had been subdivided into four members: the Hanadi, Dababiya Quarry, Mahmiya, and Abu Had Members. Five calcareous nannofossil biozones (NP7/8, NP9 to NP12) and four subzones (NP9a and NP9b and NP10a and NP10b) were recognized. The lowest occurrences (LOs) of *Fasciculithus alanii* group, *Neochiastozygus junctus*, *Sphenolithus radians*, and *Blackites herculesii* as well as the highest occurrence of *F. alanii* group and the increased frequency of *N. junctus* are biostratigraphically significant. On contrast, the LOs of *Discoaster binodosus*, *Discoaster mahmoudii*, *Discoaster diastypus*, *Zygrhablithus bijugatus*, and *Campylosphaera dela* as well as the LOs of *Fasciculithus tympaniformis* are unreliable bio-events. Calcareous nannofossils increase in abundance close to the P–E transition. *Ericsonia subpertusa* suddenly increases above the base of Eocene, whereas the diversity of *Fasciculithus* drops close to this level. The P–E boundary at G. Nezzazat was placed at the base of the Dababiya Quarry Member in coincidence with the base of Subzone NP9b that was delineated by the LOs of *Discoaster araneus*, *Rhomboaster cuspis*, *Rhomboaster calcitrappa*, *Rhomboaster spineus*, and *Rhomboaster bitrifida*. A small gap was recorded across the P–E boundary as indicated by the lack of the four beds of the Dababiya Quarry Member. The changes in calcareous nannofossil assemblages reveal warm-water and oligotrophic conditions prevailed during the transition at G. Nezzazat.

Keywords Nezzazat · Calcareous nannofossils · Paleocene/Eocene · *Rhomboaster* · Sinai · Egypt

Responsible Editor: Zakaria Hamimi

This article is part of the Topical Collection on Current Advances in Geological Research of Egypt

✉ Fatma Shaker
FATMA.ELDESOUKY@fsc.bu.edu.eg;
felkamar@gmail.com

Atef M. Kasem
kasematef@sci.dmu.edu.eg

Mahmoud M. Faris
mhmfaris@yahoo.com

Osman M. Osman
Osmanbadran313@yahoo.com

Ahmed Yehia E. Badawy
ahmedshager555@yahoo.com

¹ Geology Department, Faculty of Science, Damanhour University, Damanhour, Egypt

² Geology Department, Faculty of Science, Tanta University, Tanta, Egypt

³ Geology Department, Faculty of Science, Benha University, Benha, Egypt

Introduction

The Paleocene–Eocene was distinguished by various climatic, sedimentologic, isotopic, and paleontologic variations (Dupuis et al. 2003). This interval was accompanied by a short-lived episode of global warming associated with negative shifts in the $\delta^{13}\text{C}$ and $\delta^{18}\text{O}$ values as well as carbonate

Fig. 1 Location map shows the study section (Gebel Nezzazat, West Central Sinai, Egypt)



Fig. 2 Google earth map, shows the study section (Gebel Nezzazat, West Central Sinai, Egypt).



Table 2 Lithostratigraphic correlation of the present study section with some previous works

Age	Beadnell (1905) (Southern Egypt)	Hume (1911) (Western Egypt)	Said (1961) (Southern Egypt)	Said (1962) (Sinai)	Awad & Ghobrial (1965) (Southern Egypt)	El Naggar (1966) (Western Egypt)	Abdel Razik (1972) (Egypt)	Hernina in Said (1990) (El Farafra)	El-Dawy & Hewaidy (2003) (Sinai)	Ayyad et al. (2003) (Sinai)	Dupuis et al. (2003) (Dababiya) (GSSP)	Faris et al. (2005 a, b) (Sinai)	Tantawy (2006) (Dababiya)	Aubry et al. (2007) (Nile Valley)	Present Study											
Eocene Ypresian	Thebes Fm.	Thebes Fm.	Thebes Fm.	Egma Fm.	Thebes Fm.	Thebes Fm.	Thebes Fm.	Naqb Fm.	Thebes Fm.	Thebes Fm.	Thebes Fm.	Thebes/Egma Fm.	Thebes Fm.	Thebes Fm.	Thebes Fm.											
	Esna Shales Passage Beds	Upper Esna Fm.	Esna Fm.		Esna Fm.	Upper Oweina Shale	El shaghab Mb.	Esna Fm.	Esna Fm.	Esna Fm.	Esna Fm.	Esna Unit III	Esna Fm.	Unit V	Abu Had Mb.	Abu Had Mb.										
															El Mahmiya	El Mahmiya										
	Esna Unit II	Dababiya Quarry	Esna Unit		Esna Fm.	Esna Fm.	Esna Unit	Esna Unit	Esna Unit	Esna Unit	Esna Unit	Esna Unit	Esna Unit	Esna Fm.	Unit I	Dababiya Mb.	Dababiya Mb.									
																Dababiya Mb.	Dababiya Mb.									
																El Hanadi	El Hanadi									
	Esna Unit I	Esna Unit	Esna Unit		Esna Fm.	Esna Fm.	Esna Unit	Esna Unit	Esna Unit	Esna Unit	Esna Unit	Esna Unit	Esna Unit	Esna Fm.	Unit I	El Hanadi	El Hanadi									
																El Hanadi	El Hanadi									
																El Hanadi	El Hanadi									
	Paleocene Thanetian	Chalk Fm.	Chalk Fm.		Chalk Fm.	Dakhla Fm.	Tarawan Fm.	Middle Oweina Chalk	Tarawan Chalk	Tarawan Fm.	Tarawan Fm.	Tarawan Fm.	Tarawan Limestone	Tarawan Fm.	Tarawan Fm.	Tarawan Fm.	Tarawan Fm.									
D-S		Lower Esna Fm.	Dakhla Fm.	Dakhla Fm.	L. Oweina		Sharawna	Beida	Dakhla Fm.	Dakhla Shale	Dakhla Shale	Dakhla Shale	Dakhla Shale	Dakhla Shale	Dakhla Shale	Dakhla Shale										
																	Kharga M.	Kharga M.								
Cret. Maa.	Maa.	Maa.	Maa.	Chalk	Dakhla Fm.	Dakhla Fm.	Dakhla Fm.	Dakhla Fm.	Dakhla Fm.	Dakhla Fm.	Dakhla Fm.	Dakhla Fm.	Dakhla Fm.	Dakhla Fm.	Dakhla Fm.											
																Dakhla Fm.	Dakhla Fm.	Dakhla Fm.	Dakhla Fm.	Dakhla Fm.	Dakhla Fm.	Dakhla Fm.	Dakhla Fm.	Dakhla Fm.	Dakhla Fm.	Dakhla Fm.

Cret. Cretaceous, Maa. Maastrichtian, D-S Danian–Selandian, Fm. Formation, Mb. Member, DQM Dababiya Quarry Member

Lithostratigraphy

The uppermost Paleocene–lowermost Eocene at Gebel Nezzazat (G. Nezzazat) extends in three formations that are, from base to top, the Tarawan, Esna, as well as Thebes Formations (Fig. 3, Table 2).

The Tarawan Formation

Awad and Ghobrial (1965) had introduced this unit to describe a succession of chalk passing into chalky limestones and marly limestone at Gebel Tarawan, Kharga Oasis (Western Desert, Egypt). About 2.3 m from the upper part of the Tarawan Formation had been investigated in this study and consists of hard, yellow argillaceous limestone grading into white chalky limestone (Figs. 3 and 4A, B). It lies conformably above the Dakhla Formation and below the Esna Formation (Fig. 4A). Depending on the calcareous nannofossils, it was assigned to the (NP7/8 Zone) Thanetian Age (Figs. 3 and 5).

The Esna Formation

The Esna Shale Passage Beds was originally established by Beadnell (1905) to characterize a succession of 104-m-thick greenish gray shale intercalated with calcareous interbeds, grades upward into argillaceous limestone, and overlies the Cretaceous sequence and underlies the Eocene succession

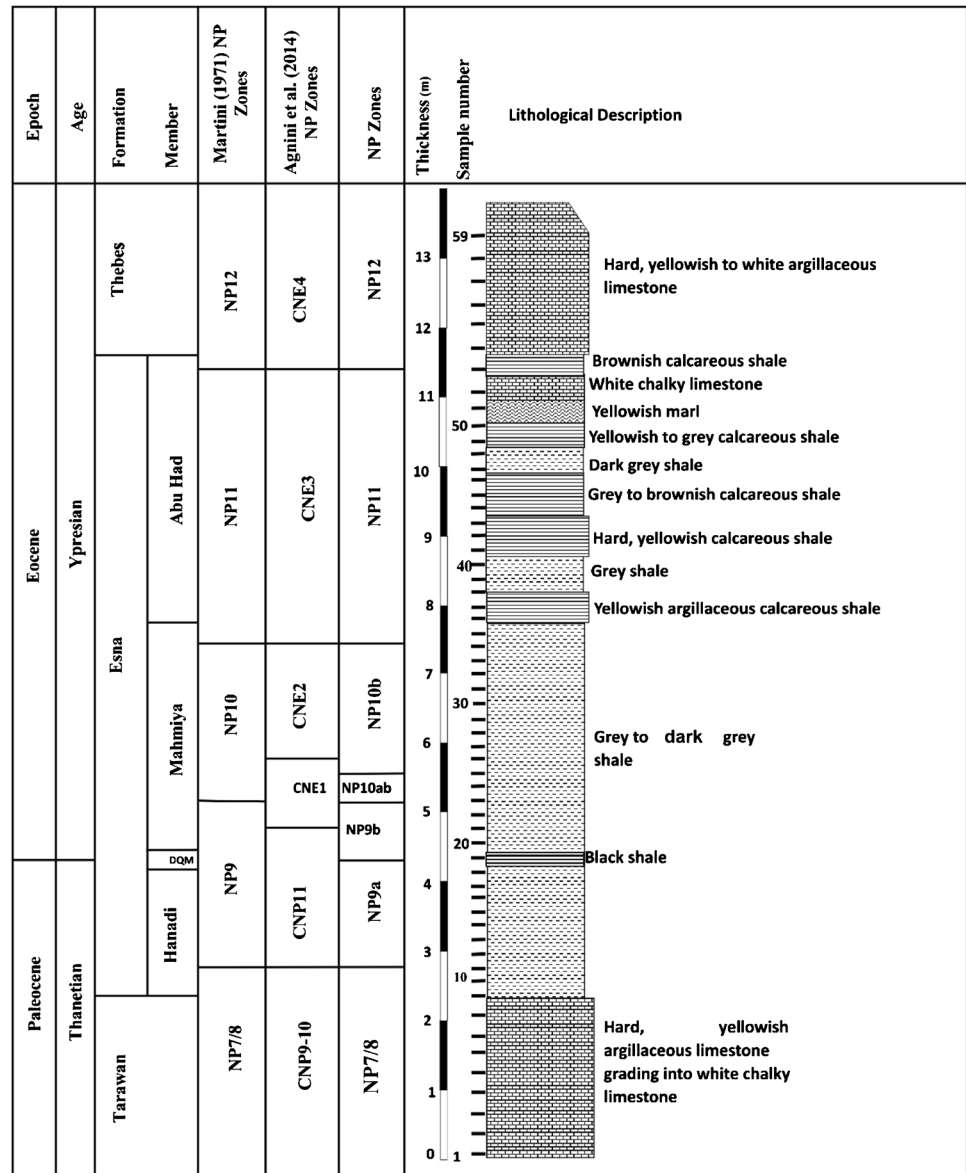
at Gebel Oweina, near Esna, southern Egypt. He named it Esna Shale. This unit was assigned to the Esna Formation by Said (1960). At G. Nezzazat, this unit is about 9.2 m of gray to dark gray shale intercalated with black shale and yellow, gray to brown calcareous shale, and upgrades to yellow marl and white chalky limestone (Figs. 3 and 4A, C, D). It conformably overlies the Tarawan Formation and is overlain by the Thebes Formation conformably (Fig. 4A, C, D). The Esna Formation in our study contains the following calcareous nannofossil biozones (the upper part of NP7/8, NP9, NP10, and NP11 and the lower part of NP12), so it is assigned to Thanetian–Ypresian ages (Figs. 3 and 5).

It was further subdivided into smaller units (e.g., Abdel Razik 1972; Dupuis et al. 2003; Tantawy 2006a, b; Ouda et al. 2016a, b; Kasem et al. 2020a, b) (Table 2). In this study, we followed the Esna Formation subdivision of Aubry et al. (2007), from base to top as follow.

The Hanadi Member

This unit was originally established to extend from the ground of the Esna Formation (Fm) to the top of the phosphatic bed (Abdel Razik 1972). Later, Aubry et al. (2007) delimit this unit to extend from the base of the Esna Fm to the base of the phosphatic bed. It consists mainly of gray, massive, calcareous shales. At G. Nezzazat, this member consists of 1.8-m-thick gray to dark gray shale (Fig. 3).

Fig. 3 Lithostratigraphic columnar section of the upper Paleocene-lower Eocene succession at G. Nezzazat, WC Sinai, Egypt.



The Dababiya Quarry Member

It was originally established by Aubry et al. (2007) to distinguish the distinct beds that mark the base of the Eocene at the Dababiya Quarry area in Egypt. These marker beds reflect climatic changes in the southern Tethys during the P-E transition as indicated by their lithological, geochemical, and biotic characteristics (Aubry et al. 2007). The base of this unit in this study is coincident with the entry of Sub-zone NP9b (Fig. 3) (Dupuis et al. 2003; Kasem et al. 2020b).

Further subdivision of these beds was introduced by several authors depending on their color, texture, contents of carbonate and coprolite, and/or the composition and patterns of foraminifers (e.g., Aubry et al. 2007; Ouda et al. 2013). Moreover, Tantawy (Tantawy 2006a, b) subdivided

the interval of the Esna Formation that covers the Dababiya Quarry Member of Aubry et al. (2007) into five units (DQB1–5). The DQB1, at section E, which lies east of the P-E GSSP is missed (Khozyem et al. 2015). At Naqb Assiut section, Kharga Oasis, Western Desert, Egypt, the Dababiya Quarry Member is only represented by the upper two beds (nos. 4 and 5) (El-Dawy et al. 2016), while at Gaga section, Baris Oasis, Western Desert, Egypt, the first bed (clay layer) of the Dababiya Quarry Member at the Paleocene/Eocene GSSP which represents the onset of the P-E boundary is missing, whereas the rest of the beds (nos. 2–4) are well represented (Metwally and Mahfouz 2018). In the present study, the Dababiya Quarry Member (DQM) is represented by only one sample of black shale, which may represent DQB1, of about 15 cm thick (Fig. 3).

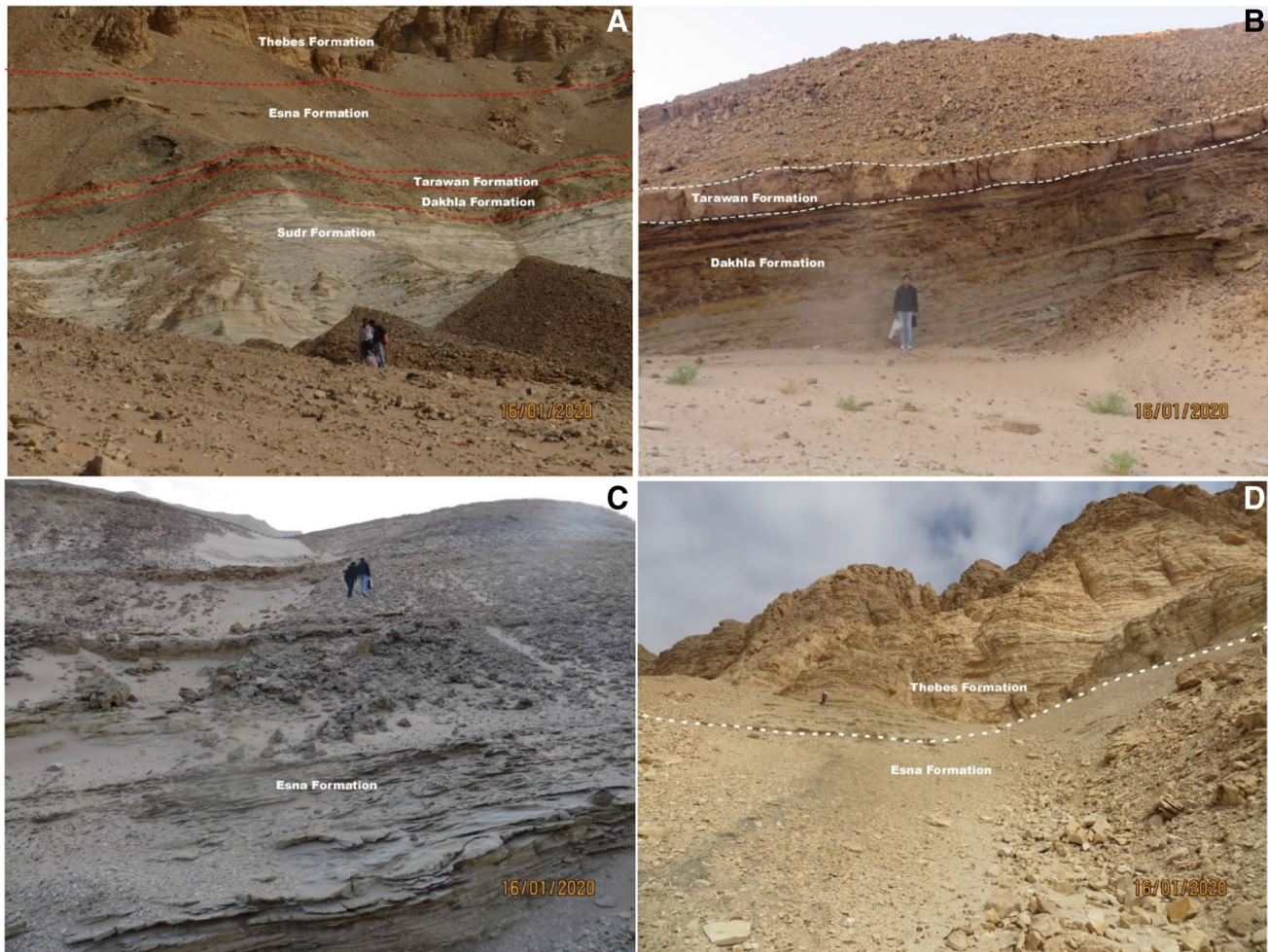


Fig. 4 A: Field photograph shows different formations covers the study interval at the study section; B: Field photograph shows the contact between Dakhla and Tarawan formations; C: Field photo-

graph shows the lower part of the Esna Formation; D: Field photograph shows the contact between the Esna and Thebes formations.

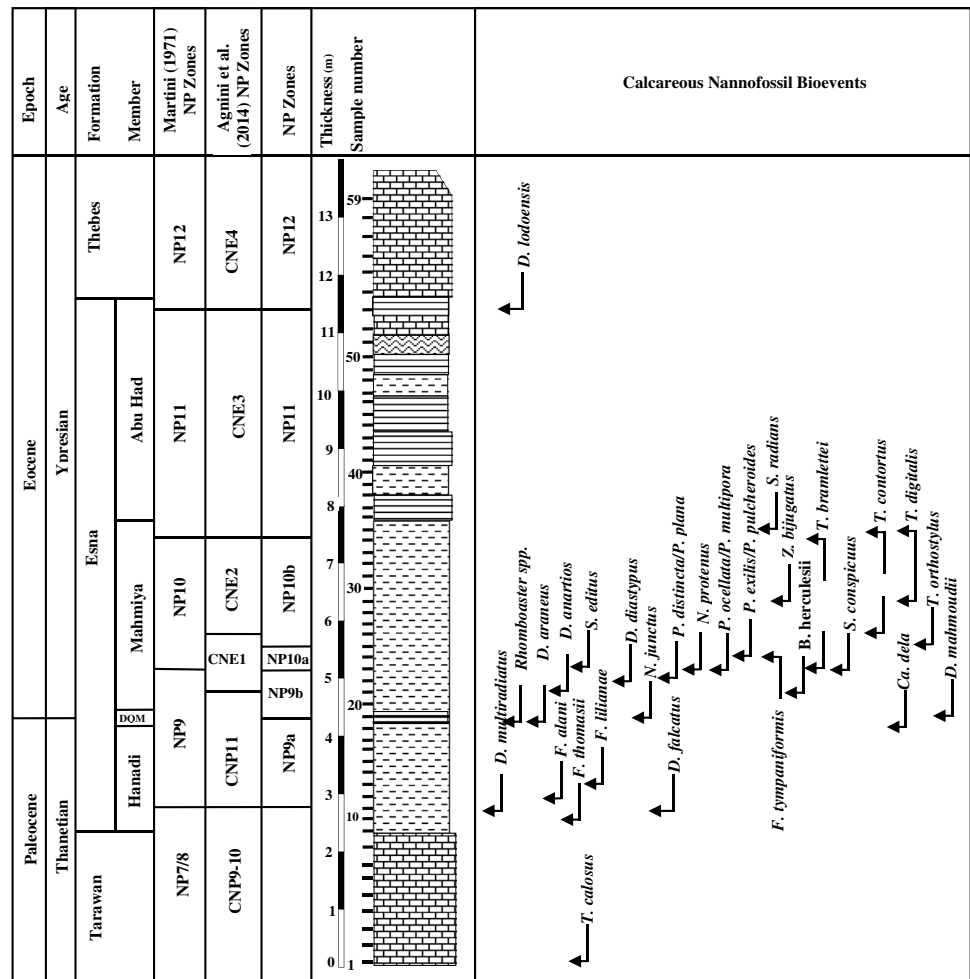
The Mahmiya Member

Aubry et al. (2007) established this member to cover the main part of the Esna Unit 2 of Dupuis et al. (2003) at the Dababiya Quarry section. It consists of monotonous, dark, clayey shales without marked bedding and has low calcium carbonate content (<50%) and clear cyclic color variations. The thickness of the Mahmiya Member is 65 m in the Dababiya Quarry section. Aubry et al. (2007) used the term El Quda Bed to describe the thin (10–30 m) calcarenite bed within the Mahmiya Member which consists generally of accumulations of cylindrical coprolites, phosphatic and shell clasts, and a variable amount of glauconite at the base (Table 2). It differs from the beds of the DQM by the presence of glauconite and the erosive and bioturbated contact with the underling lithology. In this study, the Mahmiya Member is ~3.4 m of gray to dark gray shales (Fig. 3).

The Abu Had Member

This member was originally established by Abdel Razik (1972) as the lower member of the Thebes Formation and covers the interbeds of limestones and shales at the transition between the shales of the Esna Formation and the massive carbonates of the Thebes Formation. Aubry et al. (2007) assigned this member to the Esna Formation at the Dababiya Quarry (Table 2). At the Dababiya Quarry, this member is 43.5 m thick of alternating shales and limestone. In the present study, the upper fraction of the Esna Formation at the G. Nezzazat section is assigned to the Abu Had Member and is about 4 m of yellow calcareous shale, gray shale, gray to brownish calcareous shale, dark gray shale, yellow to gray calcareous shale, yellow marl, white chalky limestone associated with chert nodules and bands, as well as brown calcareous shale (Fig. 3).

Fig. 5 Significant calcareous nannofossil bioevents of the upper Paleocene-lower Eocene succession at G.Nezzazat, WC Sinai, Egypt.



The Thebes Formation

It was described by Said (1960) to cover a 290-m white to grayish white limestone with chert bands that superimpose the Esna Formation at the Gebel Gurnah, southern Egypt. About 2 m of hard yellow to white argillaceous limestone from the lowermost part of this formation was examined at G. Nezzazat and was assigned to the Ypresian Age based on the presence of the calcareous nannofossil biozone (NP12) (Figs. 3, 4A, D, and 5). It conformably underlain by the Esna Formation.

Results

Calcareous nannofossil biostratigraphy

Martini’s (1971) zonation scheme of the Paleogene was adopted in this study, and Romein’s (1979) recommendation of combining Zones NP7 and NP8 was followed. In addition, Aubry et al.’s (1999) proposition of subdividing Zone NP9 into Subzones NP9a and NP9b was applied. Furthermore,

the subdivision of Zone NP10 suggested by Kasem et al. 2020a into Subzones NP10a and NP10b was followed. The stratigraphic importance of calcareous nannofossil bioevents that associate the P-E transition was discussed in this study. Abbreviations that are applied in this study are LO for the lowest occurrence, HO for the highest occurrence, LCO for the lowest common occurrence, and HCO for the highest common occurrence (Kasem et al. 2017b). Table 1 shows the counts and stratigraphic distributions of calcareous nannofossil assemblages. Microphotographs of the recorded species are shown in Plates 1 and 2. Five calcareous nannofossil zones and four subzones were recognized and discussed as follows.

Discoaster mohleri Zone (NP7/8)

This combined zone spans from the LO of taxon *Discoaster mohleri* to the LO of *Discoaster multiradiatus* (Romein 1979). It is comparable to Zones CP6 and CP7 of Okada and Bukry (1980) and Zones CNP9 and CNP10 of Agnini et al. (2014). Originally, it was introduced by Hay (1964), yet the

marker species *Heliolithus riedelii* was not recorded from several sections besides having inconsistent stratigraphic ranges (Perch-Nielsen 1985; Romein 1979; Agnini et al. 2007b). Accordingly, Romein (1979) excluded this bioevent from being a zonal marker and lumped Zones NP7 and NP8 together into the *D. mohleri* Zone (NP7/8). In this study, this zone is ~2.8 m thick (samples 1 to 11) and covers almost the whole Tarawan Formation and extends to the basal part of the Esna Formation (Table 1, Fig. 2). It was assigned to Thanetian.

Discoaster multiradiatus Zone (NP9)

This zone had been established by Bramlette and Sullivan (1961) and then had been emended by Martini (1971) to the biostratigraphic interval between the LOs of *Discoaster multiradiatus* and *Tribrachiatum bramlettei*. It is comparable to Zone CN8 of Okada and Bukry (1980), Subzone NTP16b to Zone NTP20 of Varol (1989), and Zone CNP11 plus the lower part of Zone CNE1 of Agnini et al. (2014). Zone NP9 was documented from several Paleocene–Eocene successions in Egypt (Kasem et al. 2020a, b). At G. Nezzazat, this zone extends from sample 11 to sample 22 and is ~2.4 m thick in the basal portion of the Esna Formation and dates Thanetian–Ypresian (Table 1, Fig. 3).

Most *Discoaster* species that mark the Paleocene first occur in this zone, and genera *Fasciculithus* and *Rhomboaster* radiate in this zone (Table 1). Furthermore, many species belonging to the genus *Fasciculithus* disappear in the upper part of this zone (Table 1), among them are, e.g., *Fasciculithus lillianae*, *Fasciculithus alanii*, *Fasciculithus thomasii*, and *Fasciculithus clinatus*. Further subdivisions of Martini's (1971) Zone NP9 or equivalent interval had been recommended by several authors (Bukry 1973; Varol 1989; Kasem et al. 2020a, b).

Bukry (1973) subdivided this interval (Zone CP8) based on the LO of *Campylosphaera eodela*, *Rhomboaster cuspis*, and related taxa in shallow-ocean areas, and by *C. eodela* in deep-ocean areas (Bukry and Percival 1971). This subdivision is consistent with the occurrences documented by many authors (e.g., Tantawy 2006a, b). However, later studies confirmed that *Campylosphaera eodela* has taxonomic disputes and inconsistent stratigraphic ranges and, thus, is an unreliable zonal marker (Agnini et al. 2007b; Kasem et al. 2020a, b).

Bybell and Self-Trail (1997) further subdivided Zone NP9 based on the HOs of fasciculithus species (e.g., *F. clinatus*, *F. lillianae*, *Fasciculithus hayi*, *Fasciculithus bobii*, *F. alanii*, and *Fasciculithus mitreus*). Yet Khozyem et al. (2013) noted that these species disappear within Zone NP9. Furthermore, Kasem et al. (2020b) recorded *Fasciculithus involutus* plus

Fasciculithus tympaniformis in the basal portion of Zone NP10. Aubry et al. (1999) suggested subdividing Zone NP9 into two subzones (NP9a and NP9b), relying on the LOs of genus *Rhomboaster*, *Discoaster araneus*, plus/or *Discoaster anartios*. Several studies confirmed the applicability of this suggestion (e.g., Dupuis et al. 2003; Agnini et al. 2007a, b; Faris et al. 2015; Kasem et al. 2020a, b). In this study, Zone NP9 has been subdivided into two subzones as follows.

NP9a Subzone

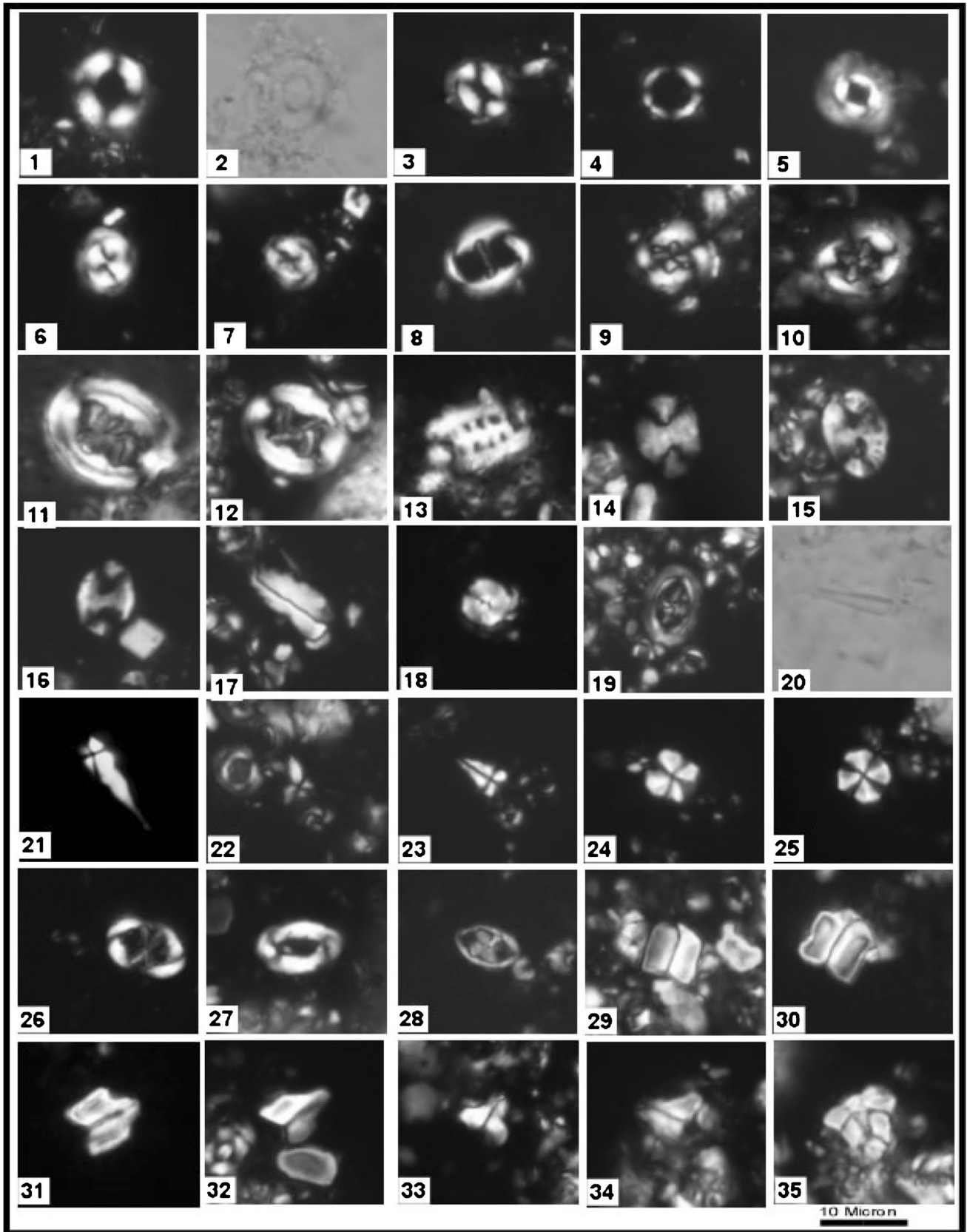
It covers the biostratigraphic interval between the LOs of *Discoaster multiradiatus* and *Rhomboaster* spp., *D. araneus*, plus/or *D. anartios* (Aubry et al. 1999). It extends from sample 11 to sample 18 at G. Nezzazat (Table 1) and covers about 1.5 m in the lower portion of the Esna Formation (Fig. 3). This subzone belongs to the Thanetian Age. Several new species come in this interval; among them are *Fasciculithus lillianiae*, *Neochiastozygus pusillus*, *Ellipsolithus distichus*, *Discoaster barbadiensis*, *Discoaster falcatus*, *Neochiastozygus distentus*, and *Lanternithus simplex* (Table 1).

NP9b Subzone

The base of this subzone was located by the LOs of *Rhomboaster* spp., *D. araneus*, and/or *D. anartios*, and its upper limit was delineated by the LO of taxon *Tribrachiatum bramlettei* (Aubry et al. 1999). It is 0.9 m thick in the Esna Fm at G. Nezzazat (Fig. 3), covering from sample 19 (black shale) to sample 22, and belongs to the Ypresian Age (Table 1). Many new species first occur in this interval; among them are *Rhomboaster cuspis*, *Rhomboaster spineus*, *Rhomboaster bitrifida*, *Rhomboaster calcitrapa*, *Chiasmolithus nitidus*, *Discoaster mahmoudii*, *D. araneus*, *D. anartios*, *Calcidiscus* sp., *Blackites herculesii*, *Discoaster diastypus*, *Pontosphaera plana*, and *Pontosphaera distincta* (Table 1). The HO of *Fasciculithus alanii* as well as the LOs of *Rhomboaster calcitrapa*, *Rhomboaster intermedia*, and *Blackites herculesii* were used to delineate the lower limit of Subzone NP9b (Faris and Salem 2007). Some authors documented that *Fasciculithus alanii* go extinct in coincidence with the ground of Subzone NP9b (Faris and Salem 2007), yet it has its HO earlier at the Dababiya Quarry (Dupuis et al. 2003), and extend up to the lowermost Eocene in some sections (Kasem et al. 2020b). In this study, *F. alanii* occurs in Subzone NP9b (Table 1).

Tribrachiatum contortum Zone (NP10)

Hay (1964) reported that this biozone covers from the LO of *Tribrachiatum bramlettei* to the HO of *T. contortum*. This zone is comparable to Subzone CP9a of Okada and Bukry



◀**Plate 1** 1, 2 *Coccolithus formosus*. Sample No. 57, Zone NP12. 3 *Coccolithus pelagicus*. Sample No. 6, Zone NP7/8. 4 *Ericsonia robusta*. Sample No. 14, Subzone NP9a. 5 *Toweius callosus*. Sample No. 55, Zone NP12. 6 *Toweius eminens*. Sample No. 21, Subzone NP9b. 7 *Toweius pertusus*. Sample No. 11, Zone NP9a. 8 *Lophodolichus nascens*. Sample No. 57, Zone NP12. 9 *Cruciplacolithus tenuis*. Sample No. 11, Zone NP9a. 10 *Chiasmolithus consuetus*. Sample No. 21, Subzone NP9b. 11 *Chiasmolithus grandis*. Sample No. 30, Subzone NP10b. 12 *Chiasmolithus bidens*. Sample No. 22, Subzone NP9b. 13 *Ellipsolithus distichus*. Sample No. 21, Subzone NP9b. 14 *Ellipsolithus macellus*. Sample No. 44, Zone NP11. 15 *Pontosphaera pulcheroides*. Sample No. 51, Zone NP11. 16 *Pontosphaera exilis*. Sample No. 47, Zone NP11. 17 *Zygrhablithus bijugatus*. Sample No. 44, Zone NP11. 18 *Bomolithus elegans*. Sample No. 11, Zone NP9a. 19 *Campylosphaera dela*. Sample No. 57, Zone NP12. 20 *Blackites herculesii*. Sample No. 23, Subzone NP9b. 21 *Sphenolithus villae*. Sample No. 41, Zone NP11. 22 *Sphenolithus editus*. Sample No. 47, Zone NP11. 23 *Sphenolithus radians*. Sample No. 57, Zone NP12. 24 *Sphenolithus primus*. Sample No. 51, Zone NP11. 25 *Bomolithus conicus*. Sample No. 44, Zone NP11. 26 *Neochiastozygus junctus*. Sample No. 21, Subzone NP9b. 27 *Neochiastozygus distentus*. Sample No. 20, Subzone NP9b. 28 *Neococcolithes protenus*. Sample No. 57, Zone NP12. 29 *Fasciculithus tympaniformis*. Sample No. 11, Zone NP9a. 30 *Fasciculithus billii*. Sample No. 11, Zone NP7/8. 31, 32 *Fasciculithus lillianaiae*. Sample No. 15, Subzone NP9a. 33, 34 *Fasciculithus alanii*. 33, Sample No. 15, Subzone NP9a; 34, Sample No. 14, Subzone NP9a. 35 *Lithoptychius janii*. Sample No. 11, Zone NP9a

(1980) and the upper part of Zone CNE1 and Zone CNE2 of Agnini et al. (2014). It extends from sample 23 to sample 34 (~2.3 m thick) in the Esna Fm (Fig. 3) and is assigned to the Ypresian Age.

The start of Zone NP10 was delineated variously by different authors because of the taxonomic disputes among them concerning whether *T. bramlettei* has a different structure from *Rhomboaster* or not (Kasem et al. 2020a). Faris et al. (2015) proposed to locate the base of Zone NP10 at the LCO of *T. bramlettei*. At G. Nezzazat, *T. bramlettei* first occurs in sample number 23 with common occurrence (Table 1) and has been adopted to mark the base of Zone NP10. Abu Shama et al. (2007) suggested approximating the base of Zone NP10 at the increased frequency of *Neochiastozygus junctus* to delineate the lower limit of Zone NP10. At G. Nezzazat, *N. junctus* first occurs in sample 19 and shows increased frequency in sample 21 slightly below the base of Zone NP10 (sample 23) (Table 1).

The genus *Fasciculithus* commonly disappears in the basal part of Zone NP10 (Romein 1979); thus, it can help in the approximation of the lower limit of this zone in case of the scarcity or absence of the zonal marker (Perch-Nielsen 1985). However, Kasem et al. (2020a) noted that *F. tympaniformis* occurs with common occurrence up to the middle part of Zone NP10. Representatives of genus *Tribrachiatus* are important in biostratigraphic correlation and further subdivision of Zone NP10. The co-occurrences of *Tribrachiatus bramlettei* and *T. contortus* in Zone NP10 from one side and *T. contortus*–*Tribrachiatus orthostylus* from another side are

a good indicator to the completeness of this interval (e.g., Agnini et al. 2006; Kasem et al. 2020a, b).

At G. Nezzazat, an overlap between the stratigraphic ranges *T. bramlettei* and *T. contortus* which were documented extends from sample 26 to sample 33, and *T. contortus* and *T. orthostylus* have a stratigraphic overlap extending from sample 26 to sample 34 (Table 1). Some authors suggested further subdivisions for Martini's (1971) Zone NP10 (e.g., Aubry 1996; Kasem et al. 2020a).

Aubry (1996) suggested subdividing Zone NP10 into four subzones: NP10a to NP10d, based on LOs and HOs of *Tribrachiatus digitalis* and *T. contortus*. The validity of this suggestion was confirmed by various studies (e.g., Dupuis et al. 2003; Al Wosabi 2015). Yet the reliability of *T. digitalis* as a marker is questionable because of the disputes concerning its taxonomic position and biostratigraphic range (Raffi et al. 2005). Consequently, Kasem et al. (2020a, b) recommended to exclude *T. digitalis* from being a reliable subzonal marker and used the LO *T. contortus* to subdivide Zone NP10 into Subzone NP10a plus NP10b. This suggestion is followed in this study.

Subzone NP10a

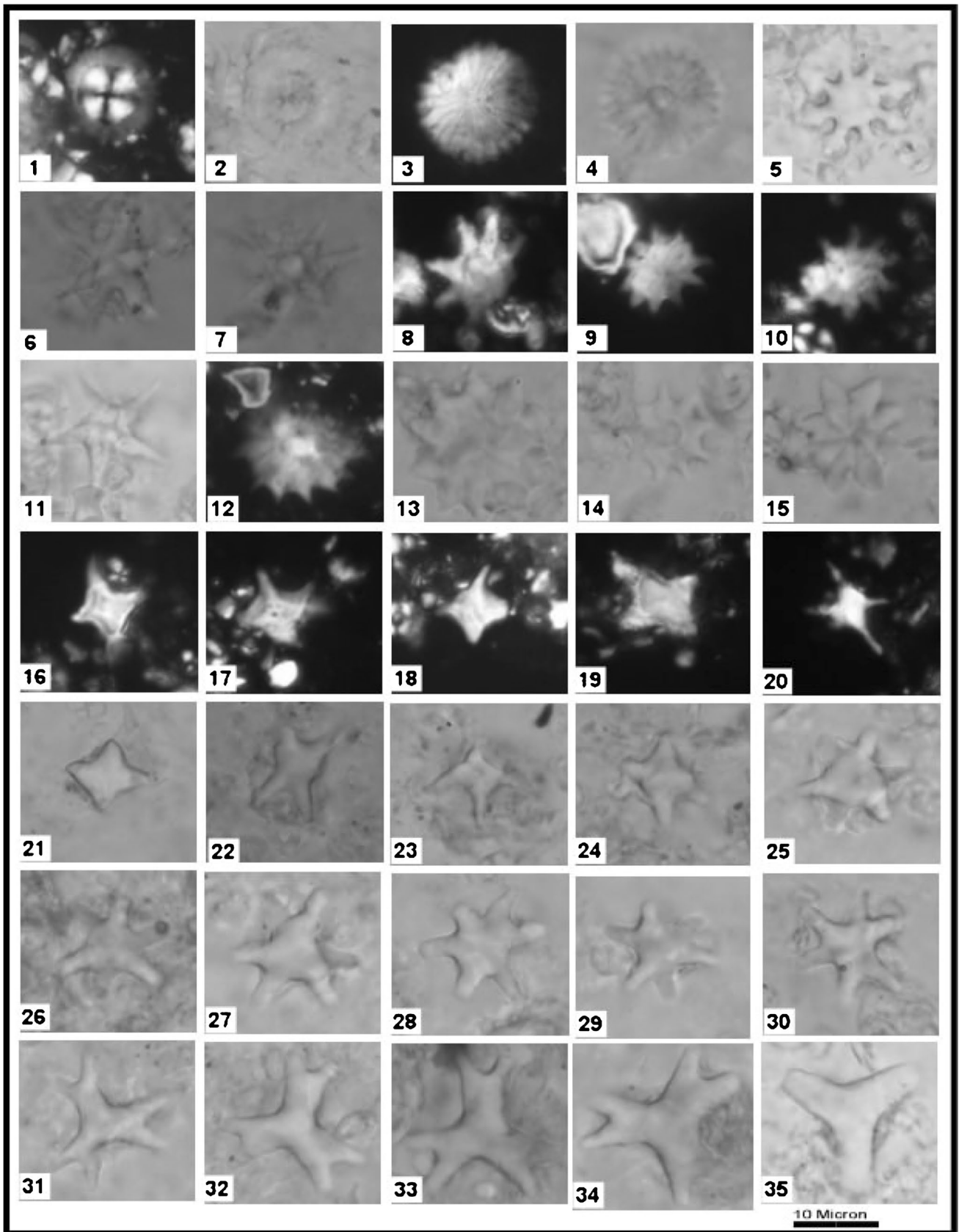
Kasem et al. (2020a) introduced Subzone NP10a to extend between the subsequent LOs of *Tribrachiatus bramlettei* and *T. contortus*. This subzone is comparable to Aubry's (1996) Subzones NP10a to NP10c and Tantawy's (1998) Subzones NP10a and NP10b. At G. Nezzazat, this subzone extends from sample 23 to sample 25 (~40 cm thick) in the Esna Formation (Fig. 3, Table 1) and is assigned to the Ypresian Age.

Subzone NP10b

Aubry (1996) introduced Subzone NP10d to cover the total range of *Tribrachiatus contortus*. Later, Kasem et al. (2020a) assigned this Subzone NP10b. This subzone is comparable to Tantawy's (1998) Subzone NP10c. It covers from sample 26 to sample 34 (~1.9 m thick) in the Esna Formation (Table 1, Fig. 3) and is assigned to Ypresian. The incoming species that appear in this interval include *Tribrachiatus digitalis*, *T. orthostylus*, *Zygrhablithus bijugatus*, and *Neochiastozygus macilentus* (Table 1).

Discoaster binodosus Zone (NP11)

This zone covers from the HO of *Tribrachiatus contortus* to the LO of *Discoaster lodoensis* as delineated by Hay and Mohler (1967). It is comparable to Subzone CP9b of Okada and Bukry (1980) and is equivalent to Zone CNE3 of Agnini et al. (2014). At G. Nezzazat, this zone is ~3.9 m thick in the Esna Formation (Table 1, Fig. 3) and is assigned to the Ypresian Age.



◀**Plate 2** 1, 2 *Bomolithus megastypus*. Sample No. 11, Zone NP9a. 3, 4 *Discoaster multiradiatus*. 3, Sample No. 21, Subzone NP9b. 4, Sample No. 15, Subzone NP9a. 5 *Discoaster binodosus*. Sample No. 47, Zone NP11. 6–8 *Discoaster araneus*. Sample No. 19, Subzone NP9b. 9, 10 *Discoaster anartios*. Sample No. 21, Subzone NP9b. 11 *Discoaster mahmoudii*. Sample No. 22, Subzone NP9b. 12 *Discoaster diastypus*. Sample No. 20, Subzone NP9b. 13, 15 *Discoaster falcatus*. Sample No. 14, Subzone NP9a. 14 *Discoaster mediosus*. Sample No. 23, Subzone NP9b. 16–19, 21 *Rhombaster cuspis*. 16–18, Sample No. 19, Subzone NP9b; 19, Sample No. 21, Subzone NP9b; 21, Sample No. 23, Subzone NP9b. 20 *Rhombaster calcitrata*. Sample No. 19, Subzone NP9b. 22–24 *Rhombaster bitrifida*. 22, Sample No. 30, Subzone NP10b; 23, 24, Sample No. 23, Subzone NP9b. 25, 26 *Tribrachiatus bramlettei*. Sample No. 30, Subzone NP10b. 27–30 *Tribrachiatus contortus*. Sample No. 30, Subzone NP10b. 31–34 *Tribrachiatus digitalis*. Sample No. 31, Subzone NP10b. 35 *Tribrachiatus orthostylus*. Sample No. 47, Zone NP11

Tribrachiatus orthostylus commonly appear close to the base of Zone NP11 and, therefore, can approximate the entry of this zone when its zonal marker is absent (Perch-Nielsen 1985). In this study, *T. orthostylus* appears with sporadic occurrence at the base of Subzone NP10b; however, its lowest continuous occurrence (LCtO) and increased frequency are coincident with the base of Zone NP11 (sample 35) (Table 1). Moreover, the LCtO and increased frequency of *T. orthostylus* are coincident with the LO of *Sphenolithus radians* (Table 1) and can approximate the entry of Zone NP11 when *T. contortus* is absent (Raffi et al. 2005; Kasem et al. 2020a).

Tribrachiatus orthostylus Zone (NP12)

It ranges from the LO of *Discoaster lodoensis* to the HO of taxon *Tribrachiatus orthostylus* (Brönnimann and Stradner 1960). It is correlative to Okada and Bukry's (1980) Zone CP10 and Zone CNE4 of Agnini et al. (2014). It covers ~2 m from the uppermost Esna Fm to the lowermost Thebes Fm and is assigned to the Ypresian Age (Table 1, Fig. 3). In case of poor preservation of the zonal marker, the base of Zone NP12 can be placed approximately based on the LOs of *Sphenolithus conspicuus* that often first occurs in the topmost of Zone NP11 and the LO of *Neococcolithus dubius* that commonly first occurs in the lowermost of Zone NP12 (Abu Shama et al. 2007).

Discussion

The latest Paleocene–earliest Eocene interval was characterized by biotic and lithological changes (Dupuis et al. 2003). These variations are important in limiting the P-E boundary and biostratigraphic purposes (Bukry 1973; Aubry 1996; Kasem et al. 2020a, b, etc.).

Calcareous nannofossil bioevents

Considerable changes in calcareous nannofossils are associating the Paleocene–Eocene Thermal Maximum (PETM) and are useful for the placement of the P-E boundary (Romein 1979; Dupuis et al. 2003; Raffi et al. 2005; Agnini et al. 2007a, b). These changes include incoming of new species, radiations, migration towards higher latitudes, and turnovers of some taxa (Kasem et al. 2020a, b).

Several authors tracked the variations in calcareous nannofossil assemblages that associated the PETM in Egypt (e.g., Dupuis et al. 2003; Tantawy 2006a, b; Abu Shama et al. 2007; Abu 2020; Faris and Abu Shama 2007; Berggren et al. 2012; Youssef 2015; Faris and Farouk 2015; Faris et al. 2017; Faris et al. 2014; Faris et al. 2018; Youssef 2015, 2016; Kasem et al. 2020a, b). According to these studies, the P-E boundary was delineated either in Zone NP9, at the base of Zone NP10 or within Zone NP10 (Kasem et al. 2020a, b; Table 3). The biostratigraphic importance of calcareous nannofossil bioevents that predate, coincide, and postdate the P-E transition is discussed below (Fig. 5).

The LO and HO of *Discoaster multiradiatus*

Discoaster multiradiatus had been regarded as a reliable Paleocene zonal marker by various authors (e.g., Varol 1989; Agnini et al. 2017). Moreover, this species is supposed to go extinct in the lower portion of Zone NP11 (Perch-Nielsen 1985); however, Kasem et al. (2020a) noted that it disappears in Subzone NP10b. At Nezzazat, it disappears within the upper part of Zone NP11 (Table 1). Thus, the HO of *D. multiradiatus* seems to be inconsistent and unreliable for biostratigraphic correlations.

The LO of the *Fasciculithus alanii* group

The last radiation of *Fasciculithus* occurs during the latest Paleocene (Romein 1979). Previous studies revealed that *F. alanii* first occurs in Subzone NP9a and disappears in this subzone close to the CIE (Dupuis et al. 2003; Faris and Farouk 2015). Thus, it can distinguish the Paleocene portion of Zone NP9 from the Eocene part (Aubry and Salem 2013a). However, Faris and Abu Shama (2007) recorded *F. alanii* shortly above the base of Subzone NP9b.

Agnini et al. (2007b) lumped *Fasciculithus richardii*, *F. mitreus*, *F. hayi*, and *Fasciculithus schaubii* within the *F. richardii* group. Similarly, Agnini et al. (2014, 2017) lumped *Fasciculithus* species that first appear in Zone NP9 into the *F. richardii* group. Later, Kasem et al. (2020a) recommended assigning this group to the *F. alanii* group, where the occurrence and disappearance of *F. alanii* were the most important bioevents in this interval (Agnini et al. 2007a, b; Aubry and Salem 2013a).

Table 3 Compilation of calcareous nannofossil bioevents used in delineation of the P-E boundary at various localities in Egypt and the present study

Section	Location	Author	P-E boundary	Calcareous nannofossil bioevents
Gebel Nezzazat	WC Sinai	Present study	NP9a/NP9b	LOs of <i>D. araneus</i> and <i>Rhomboaster</i> spp.
Farafra-Bahariya asphaltic road	Western Desert	Kasem et al. (2020b)	NP9a/NP9b	LOs of <i>Rhomboaster</i> spp.
G. Misheiti	Central Sinai	Kasem et al. (2020b)	NP9a/NP9b	LOs of <i>D. araneus</i> , <i>D. anartios</i> , and <i>Rhomboaster</i> spp.
G. Naqp Assiut and G. Umm El Ghanayim	Kharga Oasis	Faris et al. (2017)	NP9a/NP9b	LOs of <i>D. araneus</i> and <i>Rhomboaster</i> spp.
Taramsa	West Qena	Youssef (2016)	NP9a/NP9b	LOs of <i>D. araneus</i> , <i>D. anartios</i> , <i>Discoaster aegyptiacus</i> , <i>Rhomboaster</i> spp., and <i>C. eodela/dela</i>
Duwi	Quseir			
Qeryia	Wadi Qena			
Arras	Safaga			
G. Matulla	Sinai	Faris and Farouk (2015)	NP9a/NP9b	LOs of <i>D. araneus</i> , <i>D. anartios</i> , and <i>Rhomboaster</i> spp.
G. Markha				
G. Duwi	Eastern Desert			
G. El-Qus Abu Said	Farafra Oasis			
W. Nukhul	Central Sinai	Al Wosabi (2015)	NP9a/NP9b	LOs of <i>Rhomboaster</i> spp.
Nag El-Quda	Upper Nile Valley	Youssef (2015)	NP9a/NP9b	LOs of <i>D. araneus</i> and <i>Rhomboaster</i> spp.
G. Ghanima	Kharga Oasis	Khalil and Al Sawy (2014)	NP9a/NP9b	LOs of <i>Rhomboaster</i> spp.
G. Matulla	Central Sinai	Abu Shama et al. (2007)	NP9a/NP9b	LOs of <i>Rhomboaster</i> spp.
G. El Misheiti	Themed area, Sinai	Faris and Abu Shama (2007)	NP9a/NP9b	The LOs of <i>D. araneus</i> , <i>Rhomboaster cuspis</i> , <i>R. calcitrapa</i> , and <i>R. bitrifida</i>
G. El Keeh				
G. Nukhul	Central Sinai	Faris and Salem (2007)	NP9a/NP9b	LOs of <i>Rhomboaster intermedia</i> and <i>R. calcitrapa</i>
W. Feiran				
El Serai	East Qena	Tantawy (Tantawy 2006a, b)	NP9a/NP9b	LOs of <i>C. eodela/dela</i> and <i>D. araneus</i>
Taramsa	West Qena			Abrupt decrease of <i>Fasciculithus</i> spp.
Dababiya Quarry (GSSP)	Nile Valley	Dupuis et al. (2003), and Aubry et al. (2007)	NP9a/NP9b	Barren interval followed by the LOs of <i>D. araneus</i> and <i>Rhomboaster</i> spp.
Teir/Tarawan	Kharga Oasis	Faris et al. (1999)	Within NP9	HOs of <i>Fasciculithus</i> spp.
Um El-Ghanayim				LOs of <i>T. bramlettei</i> and <i>D. binodosus</i>
El Sheikh Eissa	East Qena		Within NP9	HOs of <i>Fasciculithus</i> spp.
El-Homra El-Shanka	Esna			LO of <i>T. bramlettei</i>
G. El-Shaghab				LO of <i>T. bramlettei</i>
Duwi	Quseir	Tantawy (1998)	NP9a/NP9b	LO of <i>C. eodela/dela</i>
Oweina	Nile Valley			
Abu Had	Eastern Desert			
Wadi Tarfa	East Qena			

At G. Nezzazat, *F. richardii* appeared in sample 10 just below the base of Zone NP9, whereas *F. thomasii* appears in sample 10 in coincidence with the base of Zone NP9 and followed by the appearance of *F. alanii* in sample 12 then *F. lillianiae* in sample 13 (Table 1). These taxa were grouped in the *F. alanii* group and seem to be useful in the approximation of the base of Zone NP9 when its zonal marker is absent or poorly preserved.

The LOs and HOs of the calcareous nannofossil excursion taxa

Calcareous nannofossil excursion taxa (CNET) or the *Rhomboaster–Discoaster* (RD) assemblage includes *Discoaster araneus* and *D. anartios*, as well as *Rhomboaster* spp. They appear suddenly and dominate the nannofossil assemblages of the lowermost Eocene (Dupuis et al. 2003; Kahn and Aubry 2004; Bown and Pearson 2009). Kahn and Aubry (2004) included *D. falcatus*, *Bomolithus supremus*, *Coccolithus bownii*, and *Toweius serotinus* in the CNET.

The CNET which had been considered the most remarkable change in calcareous nannofossils marks the P-E boundary and points to unusual conditions prevailed during this interval (Mutterlose et al. 2007; Table 3).

The LOs of the CNET were useful for further subdivision of Zone NP9 (Aubry and Sanfilippo 1999; Agnini et al. 2007a, b; Kasem et al. 2020a, b). Yet, the lowermost Eocene (~73 cm) is marked by a drop in carbonate content and, subsequently, the dissolution of calcareous plankton at the GSSP (Dupuis et al. 2003), which make it hard to either recognize the exact LOs of the CNET or track the precise changes in calcareous nannofossil assemblages throughout the P-E transition (Raffi et al. 2005).

At G. Nezzazat, the LOs of *Rhomboaster calcitrata*, *R. cuspis*, *Rhomboaster spinosa*, and *Rhomboaster bitrifida* *Discoaster araneus* were used to differentiate the Paleocene Subzone NP9a from the Eocene Subzone NP9b (Table 1, Fig. 3). Furthermore, it was suggested to assign the interval from the HO of CNET and the top of Zone NP9 to Subzone NP9c (Aubry and Salem 2013a). In the present study, the CNET extends up the upper part of Zone NP10 (Table 1).

The LO of *Discoaster mahmoudii*

Previous studies revealed that *Discoaster mahmoudii* appears in Zone NP9 (Monechi et al. 2000; Aubry and Salem 2013b). Aubry and Salem (2013b) pointed to the restriction of the LO of *D. mahmoudii* to the top section of Zone NP9 (Subzone NP9c). However, it appears to be ~3.5 m above the base of Eocene at the Dababiya Quarry (Dupuis et al. 2003). Moreover, it was recorded within Zone NP10 at ~7 m above the CIE at G. Nezzi (Monechi et al. 2000).

At G. Nezzazat, the LO of *D. mahmoudii* is coincident with the base of Subzone NP9b (Table 1). Thus, the biostratigraphic significance of this event is weakened (Agnini et al. 2007a; Kasem et al. 2020a).

The LO of *Blackites herculesii*

This species had been introduced as *Rhabdosphaera herculea* (Stradner 1969) then emended to *Rhabdolithus solus* (Perch-Nielsen 1971) and later revised to *Blackites herculesii* (Bybell and Self-Trail 1997). It had been documented in Zone NP9 (Kasem et al. 2020a, b) and was suggested to be restrictive to the topmost of this zone (Aubry and Salem 2013a). However, it was recorded in Zone NP10 at the Misheiti section in Sinai, Egypt (Kasem et al. 2020a).

At G. Nezzazat, it appears in the topmost portion of Zone NP9b (sample 21) (Table 1). Thus, it can approximate the top of Zone NP9.

The LO of *Campylosphaera dela*

It is hard to distinguish between *Campylosphaera dela* and *C. eodela* (Bramlette and Sullivan 1961; Hay and Mohler 1967; Bukry and Percival 1971). Therefore, they were regarded as synonyms (Kasem et al. 2020a, b).

Bukry (1973) used the LO of *C. dela* in subdividing the interval equivalent to Martini's (1971) Zone NP9. However, Kasem et al. (2020a) noted this species in Zone NP7/8. Thus, the stratigraphic range of this taxon is inconsistent (Agnini et al. 2007b).

In this study, *C. dela* and *C. eodela* were viewed as a single taxon and first occurred in the topmost of NP9a (sample 18) just below the base of Subzone NP9b (Table 1). As a result of the inconsistent ranges and taxonomic disputes, *C. dela* was excluded from being a reliable biostratigraphic event (Kasem et al. 2020a).

The LO of *Discoaster binodosus*

It had been proposed to use the LO of *Discoaster binodosus* in the approximation of the top of Zone NP9 when its zonal marker, *Tribrachiatus bramlettei*, is scarce or absent (Perch-Nielsen 1985); however, the range of this taxon is inconsistent where it was recorded in the lower part of Zone NP9 (Faris and Salem 2007) and within Zone NP10 (Kasem et al. 2020a, b). Thus, the biostratigraphic significance of these bioevent is weakened (Faris and Salem 2007; Kasem et al. 2020a, b).

In this study, *D. binodosus* appears within Subzone NP9b, but it is sporadic in the early stage of its range and its LCO is coincident with the base of Subzone NP10b (Table 1).

The drop in the frequency and diversity of *Fasciculithus* species

Several studies documented a severe decrease in the diversity of *Fasciculithus* close to the upper limit of Paleocene (e.g., Agnini et al. 2007a, b; Kasem et al. 2020a).

In this study, the diversity of *Fasciculithus* decreases from 10 species in sample 17 slightly below the ground of Subzone NP9b into 5 and 3 just below and above the P-E boundary at G. Nezzazat (Table 1, Fig. 7). Furthermore, the abundance of *Fasciculithus/Lithoptychius* drops from 179 specimens per 50 fields of view (S/50 FOV) in sample 17 into 51 and 11S/50 FOV specimens just below and above the base of the Eocene (Table 1, Fig. 7).

The HOs of *Fasciculithus tympaniformis* and *F. alanii* group

Fasciculithus taxa diversified in the uppermost Paleocene and go extinct shortly above this interval (Martini 1971;

Raffi et al. 2005; Tantawy 2006a, b). Thus, it can approximately locate the top of Zone NP9 when the zonal marker *Tribrachiatius bramlettei* is poorly preserved or absent (Perch-Nielsen 1985).

Agnini et al. (2014, 2017) used the HO of *F. tympaniformis* to mark the upper limit of the earliest Eocene Zone CNE1. However, several *Fasciculithus* species were recorded up to Zone NP10 (Romein 1979; Bralower and Mutterlose 1995; Aubry 1996; Raffi et al. 2005; Agnini et al. 2007b).

Kasem et al. (2020a) noted that *F. tympaniformis* extends with common occurrences up to the topmost section of Zone NP10. In this study, *F. clinatus*, *F. involutus*, *Fasciculithus billii*, *Fasciculithus pileatus*, *Fasciculithus janii*, and *Fasciculithus bitectus* disappear in Zone NP9 (Table 1). However, *F. tympaniformis* occurs with common occurrences up to Zone NP9 and extends with rare and discontinuous occurrences up to Zone NP11 (Table 1), which indicates reworking of these specimens and supports the biostratigraphic reliability of its HCO rather than the HO that is an inconsistent bioevent, possibly due to the diachronous nature of the HO of this taxon or discrepancies concerning the taxonomic position of *T. bramlettei* (Tantawy 2006a, b; Kasem et al. 2020a).

Agnini et al. (2014, 2017) documented the HO of *F. richardii* group below the LOs of *Rhombaster* spp. and suggested delineating the base of the entry of the Eocene (base of Zone CNE1) based on the HO of this group. Abu Shama et al. (2007) recorded the HO of *F. alanii* in coincidence with the base of Subzone NP9b. Thus, the HO of *F. alanii* group can approximate the lower limit of Subzone NP9b when its subzonal markers are absent or poorly preserved.

In this study, the HOs of *F. lillianiae* and *F. thomasi* are coincident with the base of Subzone NP9b, whereas *F. alanii* extends within Subzone NP9b (Table 1).

The acme of *Ericsonia subpertusa*

An increased frequency of *Ericsonia subpertusa* was documented across the P-E interval (Dupuis et al. 2003; Abu Shama et al. 2007; Kasem et al. 2020a).

At G. Nezzazat, *E. subpertusa* dominates the latest Paleocene–earliest Eocene nannofossil assemblages; nevertheless, it suddenly increases from 121 S/50 FOV in samples 17 to 270 and 446 S/50 FOV just below and above the P-E boundary (Table 1).

The LO of *Discoaster diastypus*

The appearances of both *Tribrachiatius contortus* plus *Discoaster diastypus* had been regarded synchronous (Raffi et al. 2005). Therefore, Bukry (1973) used their LOs to limit the base of the *Discoaster diastypus* Zone of Bukry (1973) that is correlative to Zone CP9 of Okada and Bukry (1980).

The co-occurrences of *T. bramlettei* and *D. diastypus* were recorded in some areas in Egypt (e.g., Abu Shama et al. 2007), yet their LOs were not concurrent in other sections (Tantawy 2006a, b; Kasem et al. 2020a).

At G. Nezzazat, the LO of *D. diastypus* precedes the appearance of *T. bramlettei* (Table 1) that supports the diachronous nature of *D. diastypus* and/or *T. bramlettei*.

The LO of *Sphenolithus radians*

The appearance of *Sphenolithus radians* and the disappearance of species *Tribrachiatius contortus* were very associated; therefore, the LO of *S. radians* can approximate the entry of Zone NP11 when *T. contortus* is absent (Perch-Nielsen 1985). Kasem et al. (2020a) noted that the LOs of *S. radians* and *T. contortus* are coincident at Misheiti in Sinai, Egypt. However, *S. radians* were recorded up to the topmost of Zone NP11 (Abu Shama et al. 2007; Al Wosabi 2015).

At G. Nezzazat, the LO of *S. radians* and the HO of *T. contortus* are coincident (Table 1), which supports the reliability of this bioevents in approximation of the base of Zone NP11.

The LO of *Zygrhablithus bijugatus*

The LO of *Zygrhablithus bijugatus* at the base of Subzone NP9b was recorded (Kasem et al. 2020b). In this study, it occurs at the base of Subzone NP10b (Table 1). This indicates inconsistent LO of this taxon.

The LO and increased frequency of *Neochiastozygus junctus*

Kasem et al. (2020b) noted that *Neochiastozygus junctus* first occurs in Subzone NP9b and blooms just above the top of Zone NP9. The increased frequency of this taxon was used to limit the basis of Zone NP10 (Abu Shama et al. 2007).

At G. Nezzazat, the LO of *N. junctus* is coincident with the ground of Zone NP9b and increases in frequency in the upper section of Zone NP9 and in the lower part of Zone NP10 in this study (Table 1). Thus, this bioevent can approximate this interval in case of the absence of the zonal markers (Table 1).

The LOs and HOs of *Tribrachiatius* species

Genus *Tribrachiatius* is useful in biostratigraphic zonation (Martini 1971). Previous investigations documented that *T. bramlettei* appears slightly above the base of the Eocene (Agnini et al. 2007a, b). Yet its earliest occurrences are rare to very rare and sporadic (Agnini et al. 2007a).

Thus, Faris et al. (2015) suggested depending on the LCO of this taxon to delineate the lower limit of Zone NP10.

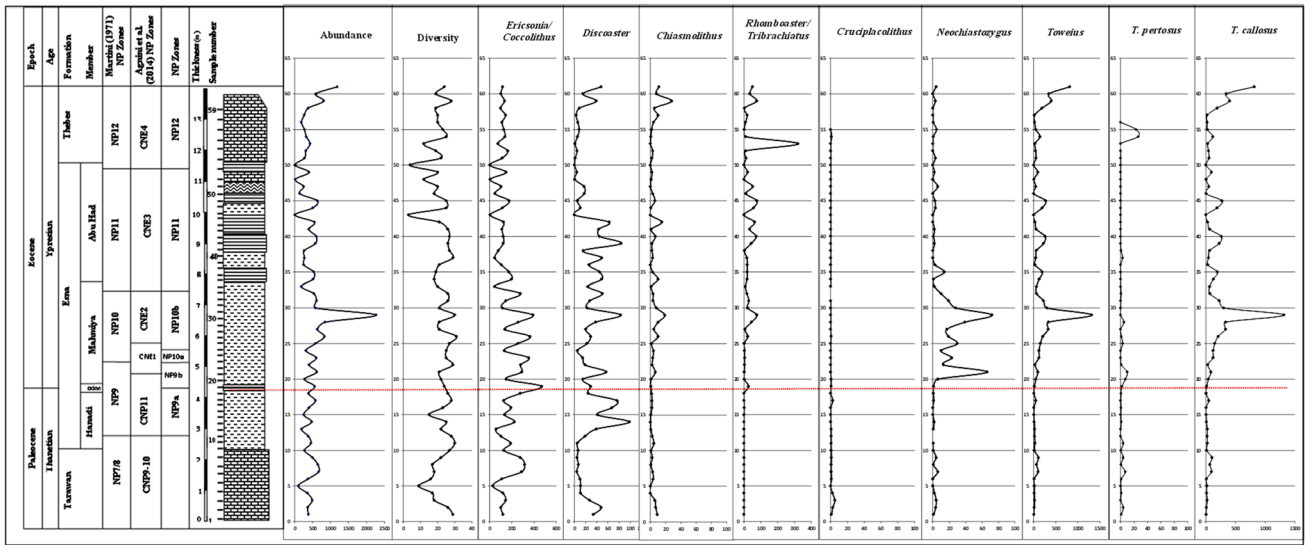


Fig. 6 Calcareous nannofossil abundance, diversity, and abundances of selected significant taxa, G. Nezzazat, WC Sinai, Egypt

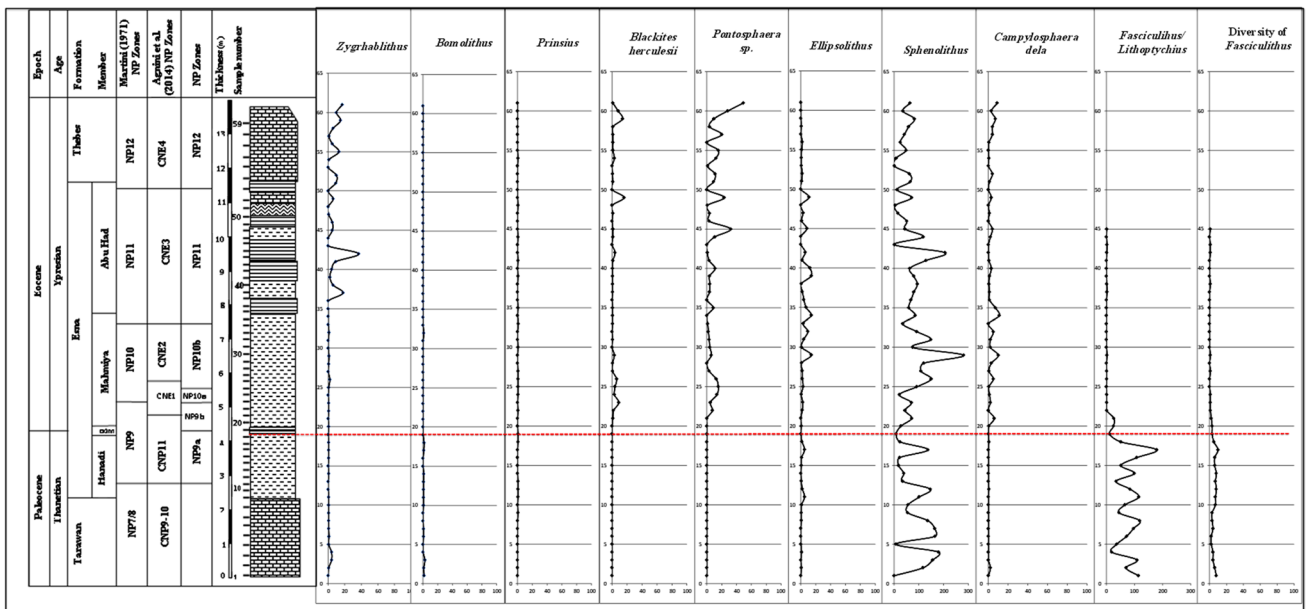


Fig.7 Abundances of selected significant calcareous nannofossil taxa, G. Nezzazat, WC Sinai, Egypt

Furthermore, the LO of *T. bramlettei* is inconsistent (Agnini et al. 2007b), probably due to the diachronous nature of this bioevent and/or dissolution that affects the lowermost Eocene sediments (Agnini et al. 2007b). In addition, *T. bramlettei* and *Rhomboaster cuspis* were considered synonyms by some authors (e.g., Von Salis et al. 2000); whereas others count them two different species (e.g., Raffi et al. 2005; Kasem et al. 2020a, b; the present study).

Furthermore, several authors reported that *Tribrachiatius bramlettei* disappears in the uppermost of Zone NP10, shortly

after the HO of *T. contortus* and below the LO of *T. orthostylus* (e.g., Aubry and Sanfilippo 1999). Nevertheless, *T. bramlettei* extends up to the top of Zone NP10 at Galala Mountains, Eastern Desert, Egypt (Marzouk and Scheibner 2003).

In this study, the HO of *T. bramlettei* occurs in sample 33 at a level somewhat below the end of Zone NP10 and slightly below the LCtO of *T. orthostylus* (Table 1).

The taxonomic position of *Tribrachiatius digitalis* underwent criticism (Raffi et al. 2005), and consequently, its biostratigraphic significance is weakened (Kasem et al.

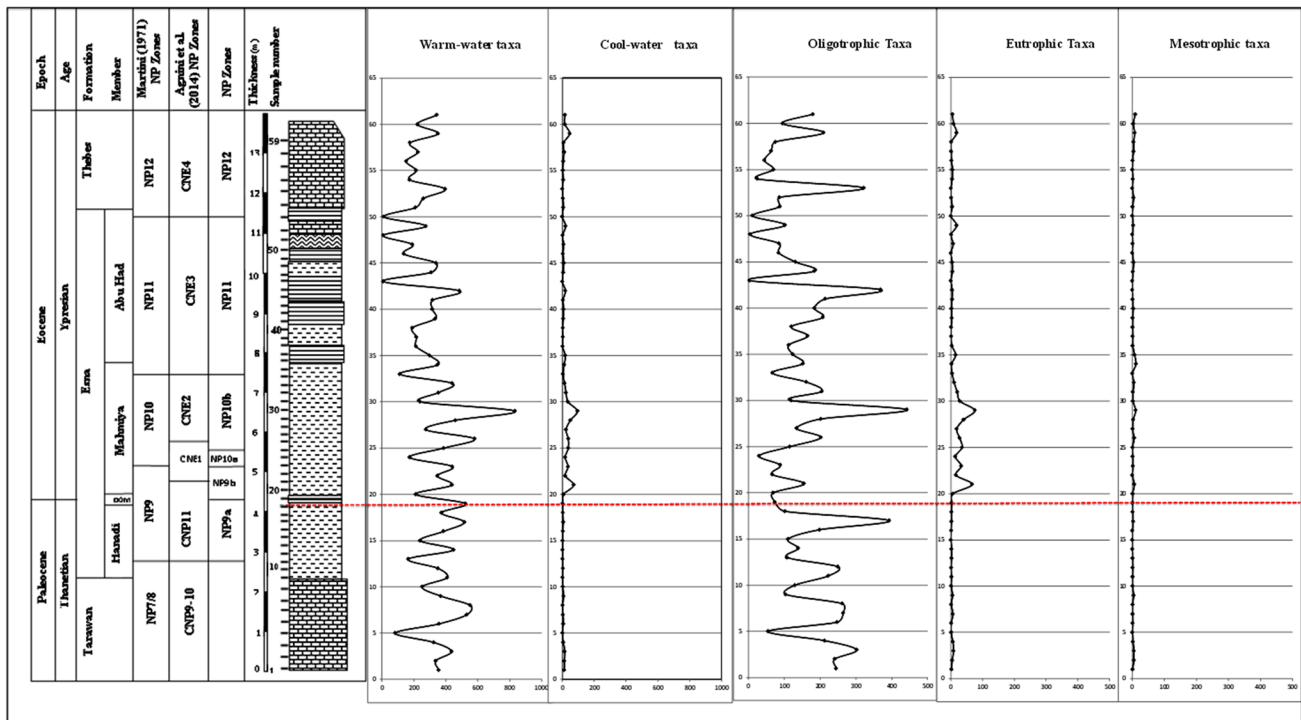


Fig. 8 Abundances of cool and warm-water taxa at G. Nezzazat, WC Sinai, Egypt

2020a, b). On the other hand, *T. contortus* is significant in biostratigraphic studies (Martini 1971), where its HO delineates the top of Zone NP10, and its LO is useful in subdividing Zone NP10 into Subzones NP10a and NP10b (Kasem et al. 2020a, b, and the present study).

The appearance of *T. orthostylus* can approximate the topmost of Zone NP10 when its zonal marker is absent (Perch-Nielsen 1985). In this study, *T. orthostylus* appears just below the base of Subzone NP10b (Table 1).

The calcareous nannofossil species richness and abundance

Calcareous nannofossils reached their maximum diversity in the Paleogene interval within Zone NP9 (Perch-Nielsen 1985). This had been confirmed in this study, where several incoming species occur in Zone NP9 such as *Discoaster falcatus*, *D. binodosus*, *Discoaster mediusus*, *D. mahmoudii*, *D. araneus*, *D. anartios*, *Discoaster lenticularis*, *D. diastypus*, *D. barbadiensis*, *Rhomboaster cuspis*, *R. calcitrapa*, *R. spineus*, *R. bitrifida*, *Fasciculithus lillianiae*, *Neochias-tozygus distentus*, *N. pusillus*, *Lanternithus simplex*, *Pontosphaera distincta*, *P. plana*, *Chiasmolithus nitidus*, *Calcidiscus* sp., *Blackites herculesii*, and *Ellipsolithus distichus* (Table 1). Nevertheless, the abundance of calcareous nannofossil assemblages shows increased frequency close to the P-E boundary (Table 1, Fig. 6).

Paleoecology

The changes in temperature and nutrient availability affect the distribution of calcareous nannofossil; therefore, they can be used for tracking climatic changes (e.g., Bralower 2002; Bernaola et al. 2007). Oligotrophic conditions with warm waters that characterize low- to middle-latitude areas are sufficient for flourishing modern calcareous nannofossil assemblages (e.g., Watkins 1989; Bralower 2002; Bornemann 2003; Fuqua et al. 2008).

On the other hand, eutrophic forms are more common in cold nutrient-rich waters at high-latitude areas (Bralower 2002). Several investigations revealed the paleoecological preferences of several calcareous nannofossil taxa (e.g., Wei and Wise Jr 1990; Fuqua et al. 2008, etc.).

In this study, the variations in paleotemperature and paleofertility were tracked depending on the changes in abundances of calcareous nannofossil species that have certain ecological preferences (Fig. 7). The taxa that had been regarded in the previously mentioned references as warm water taxa include *Ericsonia subpertusa*, *Coccolithus pelagicus*, *Fasciculithus* spp., *Lithoptychius* spp., *Discoaster* spp., *Heliolithus kleinpelli*, *Rhomboaster* spp., *Tribrachiatus* spp., *Bomolithus* spp., *Zygrhablithus bijugatus*, *Pontosphaera* spp., *Sphenolithus* spp., *Thoracosphaera operculata*, and *Thoracosphaera saxea*

(Table 1, Fig. 8) (e.g., Bukry 1973; Haq and Lohmann 1976; Abdel Hameed and Faris 1984; Roth 1986; Watkins 1989; Erba et al. 1992; Aubry 1998, 2001; Fisher and Hay 1999; Bralower 2002; Dupuis et al. 2003; Tantawy 2003, Tantawy 2006a, b, Tantawy 2011; Tremolada and Bralower 2004; Gibbs et al. 2006a, b; Mutterlose et al. 2007; Fuqua et al. 2008 and others).

Elsewhere, the taxa that had been regarded cool-water forms include *Cruciplacolithus* spp., *Neochiastozygus junctus*, *Chiasmolithus* spp., *Toweius eminens*, *Zeugrhabdotus sigmoides*, *Prinsius* spp., *Blackites herculesii*, *Markalius inversus*, *Eiffelolithus* spp., and *Neococcolithes dubius* (Table 1, Fig. 8) (e.g., Bukry 1973; Thierstein 1981; Pospichal and Wise Jr 1990; Bassiouni et al. 1991; Pospichal 1991; Firth and Wise Jr 1992; Bralower 2002; Tantawy 2003; Abu Shama et al. 2007; Fuqua et al. 2008; Monechi et al. 2013 and others).

Furthermore, the taxa regarded as oligotrophic forms in this study include *Fasciculithus* spp., *Tribrachiatus* spp., *Rhomboaster* spp., *Sphenolithus* spp., *Discoaster* spp., *Bomolithus* spp., *Heliolithus kleinpellii*, *Zygrhablithus bijugatus*, and *Octolithus* spp. (Table 1, Fig. 8) (e.g., Haq and Lohmann 1976; Wei and Wise Jr 1990; Williams and Bralower 1995; Fisher and Hay 1999; Bralower 2002; Kahn and Aubry 2004; Agnini et al. 2006; Gibbs et al. 2006a, b; Bernaola et al. 2007; Mutterlose et al. 2007; Thibault and Gardin 2007; Fuqua et al. 2008; Bown and Pearson 2009 and others). Moreover, eutrophic forms include *Zeugrhabdotus sigmoides*, *T. saxea*, *Prinsius* spp., and *Blackites* spp. (e.g., Haq and Lohmann 1976; Roth and Krumbach 1986; Bassiouni et al. 1991; Eshet and Almogi Labin 1996; Thibault and Gardin 2007), and mesotrophic taxa include *Neochiastozygus* spp., *Cruciplacolithus* spp., *Toweius eminens*, and *Campylosphaera* spp. (Table 1, Fig. 8) (e.g., Aubry 1998; Gibbs et al. 2006a; Mutterlose et al. 2007; Fuqua et al. 2008).

The changes in the latest Paleocene–earliest Eocene nanofossil assemblages indicate oligotrophic and warm conditions prevailed during this interval at G. Nezzazat, in agreement with several previous studies all over the world (e.g., Bralower 2002; Tantawy 2006; Kasem et al. 2020a, b). The distortion of the shape and asymmetry of *D. araneus* and *D. anartios* indicates unusual conditions during this interval (Bralower 2002), probably due to high CO₂ that might be resulted from a mass release of methane causing global warming (Mutterlose et al. 2007).

Remarks

The Paleocene–Eocene transition was marked by geochemical, lithological, and biotic variations (Dupuis et al. 2003). Based on calcareous nanofossils, the P-E boundary had

been placed either in Zone NP9, at the NP9/10 zonal limit, or in Zone NP10 (Martini 1971; Bukry 1973; Bolle et al. 2000). At the Dababiya Quarry section in Egypt that was ratified as the GSSP for the base of Eocene, the P-E boundary was placed at the ground of Subzone NP9b (Dupuis et al. 2003). This boundary is marked by an abrupt decrease in carbon isotope and is coincident with the base of a distinctive bed of the Dababiya Quarry Member (Aubry et al. 2007).

At G. Nezzazat, this boundary had been placed at the NP9a/NP9b subzonal boundary that is denoted by the appearances of *Discoaster araneus* and/or *Rhomboaster* spp. (Table 1). This boundary is marked by the LOs of *Rhomboaster cuspis*, *R. calcitrata*, *R. spineus*, *R. bitrifida*, *D. araneus*, and *Chiasmolithus nitidus* as well as the HOs of *Fasciculithus thomasi* and *F. lillianiae* (Table 1). In addition, this level is coincident with the base of a black shale bed assigned to the DQM (correlative to DQB 4 of Tantawy 2006,) in the lower portion of the Esna Formation (Fig. 3).

This reveals the presence of a gap represented by the missing of DQB2 to DQB5, but not detected by the calcareous nanofossils. Similar results were noted in different sections in Sinai and others in Egypt (see Aubry and Salem 2013b; Obaidalla et al. 2017; Kasem et al. 2020a, b for more discussion). Variations in calcareous nanofossil assemblages reveal warming and oligotrophic conditions prevailed during the P-E transition at G. Nezzazat in agreement with results from the GSSP as well as sections from various areas in the world (Dupuis et al. 2003; Bernaola et al. 2007; Mutterlose et al. 2007; Raffi et al. 2009; Kasem et al. 2020a, b).

Conclusions

Lithostratigraphic and calcareous nanofossil biostratigraphic investigations were carried out in this study at the Gebel Nezzazat section in Central Sinai, Egypt. The interval investigated extends throughout the Tarawan, Esna, and Thebes Formations. The Esna Formation has been partitioned into the Hanadi, Dababiya Quarry, Mahmiya, and Abu Had Members.

Five calcareous nanofossil biozones were recognized (NP7/8 through NP12). Zone NP9 had been subdivided into Subzones NP9a and NP9b depending on the LOs of *Rhomboaster* spp. and/or *Discoaster araneus*. Moreover, the LO of *T. contortus* had been used to partition Zone NP10 into Subzones NP10a and NP10b.

Exclusion of *Tribrachiatus digitalis* from being a reliable marker was recommended in this study. Stratigraphic overlaps between *T. bramlettei* and *T. contortus* as well as between *T. contortus* and *T. orthostylus* were noted, indicating the completeness of this interval. Most *Fasciculithus* taxa (*F. clinatus*, *F. involutus*, *F. billii*, *F. pileatus*, *F. janii*,

and *F. bitectus*) disappear within Zone NP9. *Fasciculithus tympaniformis* occurs with common occurrences up to the top of Zone NP9 and extends with sporadic occurrences up to Zone NP11 (Table 1), supporting the insignificance of the HO of *F. tympaniformis* in biostratigraphy.

Subsequent appearances of *F. richardii*, *F. thomasi*, *F. alanii*, and *F. lillianiae* are closely related to the base of Zone NP9. These species were grouped in the *F. alanii* group, in which the LO and HO can approximate the entry of Subzone NP9a and Subzone NP9b, respectively, when their zonal markers are absent or poorly preserved.

Furthermore, *Blackites herculesii* can approximate the top of Zone NP9. The LOs of *D. mahmoudii*, *D. binodosus*, *D. diastypus*, *Zygrhablithus bijugatus*, and *Campylosphaera dela* are not reliable bioevents in biostratigraphy. On the other hand, the LO and increased frequency of *Neochias-tozgyus junctus* can approximate the upper part of Zone NP9 and the lower part of Zone NP10.

Moreover, the LO of *S. radians* is a reliable bioevent for approximating the base of Zone NP11. *Tribrachiatulus orthostylus* appears just below the base of Subzone NP10b. The abundance of calcareous nannofossils shows an increased frequency close to the P-E boundary. *Ericsonia subpertusa* dominates the calcareous nannofossil assemblages of the examined interval and suddenly increases above the P-E boundary. On contrast, a drop in the diversity of *Fasciculithus* is closely related to the P-E transition.

The P-E boundary at G. Nezzazat was placed at the base of Subzone NP9b that is denoted by the LOs of *Discoaster araneus*, *D. anartios*, and/or *Rhombaster* spp. This boundary is coincident with the base of a black shale bed assigned to the DQM in the lower portion of the Esna Formation (Fig. 3). This reveals the presence of a small gap represented by the missing of DQB2 to DQB5. The variations in calcareous nannofossils reveal warming and oligotrophic conditions prevailed through the deposition of the upper Paleocene–lowermost Eocene at the study section.

Acknowledgements We are grateful to Prof. Dr. Sherif Farouk (Egyptian Petroleum Research Institute) for his help in the field work. Prof. Dr. Abdullah Al-Amri (Editor-in-Chief), Prof. Dr. Zakaria Hamimi (Guest Editor), and the two anonymous reviewers are thanked for carefully reading our manuscript and for their constructive comments.

Funding Open access funding provided by The Science, Technology & Innovation Funding Authority (STDF) in cooperation with The Egyptian Knowledge Bank (EKB).

Declarations

Conflict of interest The authors declare that they have no competing interests.

Open Access This article is licensed under a Creative Commons Attribution 4.0 International License, which permits use, sharing,

adaptation, distribution and reproduction in any medium or format, as long as you give appropriate credit to the original author(s) and the source, provide a link to the Creative Commons licence, and indicate if changes were made. The images or other third party material in this article are included in the article's Creative Commons licence, unless indicated otherwise in a credit line to the material. If material is not included in the article's Creative Commons licence and your intended use is not permitted by statutory regulation or exceeds the permitted use, you will need to obtain permission directly from the copyright holder. To view a copy of this licence, visit <http://creativecommons.org/licenses/by/4.0/>.

References

- Abdel Hameed AT, Faris M (1984) Changes of relative surface water temperature through the Maastrichtian-Ypresian in central Egypt. Middle East Research Centre. Ain Shams University. Earth Science, pp 1–16
- Abdel Razik TM (1972) Comparative studies on the upper Cretaceous–early Paleogene sediments on the Red Sea coast, Nile Valley and Western Desert, Egypt. 6th Arab Petroleum Congress, Algeria, 71, pp. 1–23
- Abu Shama A. M, Wanas HA, El-Nahrawy SA (2020) Calcareous nannofossil biostratigraphy of the Paleocene-lower Eocene successions in the Farafra Oasis, Western Desert, Egypt, J Afr Earth Sci, Volume 150, p. 466–484.
- Abu Shama A, Faris M, Al-Wosabi K (2007) Upper Paleocene–lower Eocene calcareous nannofossil biostratigraphy and paleoecology of Gebel Matulla section, Southwestern Sinai, Egypt. In: Proceedings of the 5th International Conference on the Geology of Africa, Assiut, Egypt, pp. 33–51
- Agnini C, Muttoni G, Kent DV, Rio D (2006) Eocene biostratigraphy and magnetic stratigraphy from Possagno, Italy: The calcareous nannofossil response to climate variability. Earth Planet Sci Lett 241(3–4), pp.815–830
- Agnini C, Fornaciari E, Rio D, Tateo F, Backman J, Giusberti L (2007a) Responses of calcareous nannofossil assemblages, mineralogy and geochemistry to the environmental perturbations across the Paleocene/Eocene boundary in the Venetian Pre-Alps. Mar Micropaleontol 63:19–38
- Agnini C, Fornaciari E, Raffi I, Rio D, Röhl U, Westerhold T (2007b) High-resolution nannofossil biochronology of middle Paleocene to early Eocene at ODP Site 1262: implications for calcareous nannoplankton evolution. Mar Micropaleontol 64:215–248
- Agnini C, Fornaciari E, Raffi I, Catanzariti R, Pälke H et al (2014) Biozonation and biochronology of Paleogene calcareous nannofossils from low and middle latitudes. Newslett Stratigr Stuttgart 47(2):131–181
- Agnini C, Monechi S, Raffi I (2017) Calcareous nannofossil biostratigraphy: historical background and application in Cenozoic chronostratigraphy. Lethaia 50:447–463
- Al Wosabi KA (2015) Calcareous nannofossils biostratigraphy and Paleocology of the late Paleocene/early Eocene of Wadi Nukhul, Westcentral Sinai, Egypt. Earth Sci 4(2):59–71
- Aubry MP (1996) Towards an upper Paleocene–lower Eocene high resolution stratigraphy based on calcareous nannofossil stratigraphy. Isr J Earth Sci 44:239–253
- Aubry MP (1998) Early Paleogene calcareous nannoplankton evolution: a tale of climatic amelioration. In: Aubry MP, Ouda K (eds) Late Paleocene–early Eocene biotic and climatic events in the marine and terrestrial record. Columbia University Press, New York, pp 158–201

- Aubry MP (2001) Provincialism in the photic zone during the LPTM. In: A.M. Ash, S.L. Wing (Eds.), *Climate and biota of the early Paleogene*. International meeting, Wyoming 6 pp
- Aubry MP, Salem R (2013a) The Dababiya Quarry Core: coccolith biostratigraphy. *Stratigraphy* 9:241–259
- Aubry MP, Salem R (2013b) The Dababiya Core: a window into Paleocene to early Eocene depositional history in Egypt based on coccolith stratigraphy. *Stratigraphy* 9:287–346
- Aubry MP, Sanfilippo A (1999) Late Paleocene–early Eocene sedimentary history in western Cuba: implications for the LPTM and for regional tectonic history. *Micropaleontology* 45:5–18
- Aubry MP, Berggren WA, Cramer B, Dupuis C, Kent DV, et al. (1999) Paleocene/Eocene boundary sections in Egypt. In: *Late Paleocene–early Eocene events from Northern Africa to the Middle East*. International Symposium in Connection with 1st International Conference on the Geology of Africa, Assiut, Egypt, pp. 1–11
- Aubry MP, Ouda K, Dupuis C, Berggren WA, Van Courvering JA, Members of the Working Group on the Paleocene/Eocene Boundary (2007) The Global Standard Stratotype-Section and Point (GSSP) for the base of the Eocene Series in the Dababiya section (Egypt). *Episodes* 30(4):271–286
- Awad GH, Ghobrial MG (1965) Zonal stratigraphy of the Kharga Oasis. Ministry of Industry, General Egyptian Organization for Geological Research and Mining, Geological Survey, Cairo, Egypt, paper no. 34: 1–77
- Bassiouni MA, Faris M, Sharaby S (1991) Late Maastrichtian and Paleocene calcareous nannofossils from Ain Dabadib section, NW Kharga Oasis. *Qatar Univ Sci Bull* 11:357–375
- Beadnell HJL (1905) The relation of the Eocene and Cretaceous systems in the Esna-Aswan Reach of the Nile Valley. *J Geol Soc Lond* 61:667–676
- Berggren WA, Alegret L, Aubry MP, Cramer B, Dupuis C, Goolaert S, Kenti D, King C, Knox R, Obaidalla N, Ortiz S, Ouda K, Abdel-Sabour A, Salemi R, Senosy M, Soliman M, Soliman A (2012) The Dababiya corehole, Upper Nile Valley, Egypt: preliminary results. *Aust J Earth Sci* 105:161–168
- Bernaola G, Baceta JI, Orue-Extebarria X, Alegret L, Martin-Rubio M, Arostegui J, Dinarès-Turell J (2007) Evidence of an abrupt environmental disruption during the mid-Paleocene biotic event (Zumaia section, western Pyrenees). *Geol Soc Am Bull* 119:785–795
- Bolle MP, Tantawy A, Pardo A, Adatte T, Burns S, Kassab A (2000) Climate and environmental changes documented in the upper Paleocene to lower Eocene of Egypt. *Eclogae Geol Helv* 93:33–51
- Bown PR, Young JR (1998) Techniques, in Bown, P.R., ed., *Calcareous nannofossil biostratigraphy*: London, Kluwer Academic, p. 16–28.
- Bornemann A (2003) Case studies of Mesozoic calcareous nannofossils: implications for paleoecology, calcareous nannofossil morphology and carbonate accumulation. PhD Thesis, Ruhr-University, Bochum, 126 pp
- Bown PR, Pearson P (2009) Calcareous plankton evolution and the Paleocene/Eocene Thermal Maximum event: new evidence from Tanzania. *Mar Micropaleontology* 71:60–70
- Bown PR, Lees JA, Young JR (2004) Calcareous nannoplankton evolution and diversity through time. In: Thierstein HR, Young JR (eds) *Coccolithophores, from molecular processes to global impact*. Springer Verlag, Berlin, pp 481–508
- Bralower TJ (2002) Evidence of surface water oligotrophy during the Paleocene-Eocene Thermal Maximum: nannofossil assemblage data from Ocean Drilling Program Site 690, Maud Rise, Weddell Sea. *Paleoceanography* 17(2):13–11
- Bralower TJ, Mutterlose J (1995) Calcareous nannofossil biostratigraphy of ODP Site 865, Allison Guyot, Central Pacific Ocean: a tropical Paleogene reference section *Proc. Ocean Drill. Program Sci Results* 143:31–72
- Bralower TJ, Premoli Silva I, Malone MJ (2002) New evidence for abrupt climate change in the Cretaceous and Paleogene: an ocean drilling program expedition to Shatsky Rise, northwest Pacific. *GSA Today* 12(11):4–10
- Bramlette MN, Sullivan FR (1961) Coccolithophorids and related nannoplankton of the Early Tertiary in California. *Micropaleontology* 7:129–188
- Brönnimann P, Stradner H (1960) Die foraminiferen und Discoasteridenzonen von Kuba und ihre intercontinental correlation. *Erdoel* 76:364–369 (in German)
- Bukry D (1973) Low latitude coccoliths biostratigraphic zonation. Initial Reports of the Deep Sea Drilling Project, vol 15. US Government Printing Office, Washington, DC, pp 685–703
- Bukry D, Percival SF (1971) New Tertiary calcareous nannofossils. *Tulane Stud Geol Paleontol* 8(3):123–146
- Bybell LM, Self-Trail JM (1997) Late Paleocene and early Eocene calcareous nannofossils from three boreholes in an onshore-offshore transect from New Jersey to the Atlantic continental rise. In Miller KG, and Snyder SW (editors), *Proceeding of Ocean Drilling Program Scientific Results, 150X (1997): College Station, TX (Ocean Drilling Program)*, pp. 91–110
- Cramer BS, Wright JD, Kent DV, Aubry MP (2003) Orbital climate forcing of $\delta^{13}C$ excursions in the late Paleocene–early Eocene (chrons C24n–C25n). *Paleoceanography* 18(21):1–21
- Dupuis C, Aubry MP, Steurbaut E, Berggren WA, Ouda K, Magioncalda R, Cramer BS, Kent DV, Speijer RP, Heilmann-Clausen C (2003) The Dababiya Quarry section: lithostratigraphy, clay mineralogy, geochemistry and paleontology. *Micropaleontology* 49:41–59
- El-Dawy M, Obaidalla NA, Mahfouz KH, Abdel Wahed SA (2016) Paleocene-Eocene transition at Naqb Assiut, Kharga Oasis, Western Desert, Egypt: Stratigraphical and paleoenvironmental inferences. *J Afr Earth Sci* 117:207–222
- Erba E, Castradori F, Guasti G, Ripepe M (1992) Calcareous nannofossils and Milankovitch cycles: the example of the Gault Clay Formation (southern England). *Paleogeogr Paleoclimatol Paleoeoc* 93:47–69
- Eshet Y, Almogi Labin A (1996) Calcareous nannofossils as paleo-productivity indicators in upper Cretaceous organic-rich sequences in Israel. *Mar Micropaleontol* 29:37–61
- Faris M, Abu Shama AM (2007) Nannofossil biostratigraphy of the Paleocene lower Eocene succession in the Thamad area, east central Sinai, Egypt. *Micropaleontology* 53(1–2):127–144
- Faris M, Farouk S (2015) Calcareous nannofossils of the Paleocene-Eocene transition in four sections from Egypt. *Turk J Earth Sci* 24:585–606
- Faris M, Salem R (2007) Paleocene-Eocene calcareous nannofossil biostratigraphy in west central Sinai, Egypt. *Proceeding of the 8th Conference of Geology of Sinai for Development Ismailia, Egypt*, pp. 1–14
- Faris M, Abd El-Hameed AT, Marzouk A, Ghandour IM (1999) Early Paleogene calcareous nannofossil and planktonic foraminiferal biostratigraphy in Central Egypt. *Neues Jb Geol Paläontol Abh* 213(2):261–288
- Faris M, Abdelghany O, Zahran E (2014) Upper Maastrichtian to Lutetian nannofossil biostratigraphy, United Arab Emirates, west of the Northern Oman Mountains. *J Afr Earth Sci* 93:42–56
- Faris M, Ghandour IM, Zahran E, Mosa G (2015) Calcareous nannoplankton changes during the Paleocene-Eocene Thermal Maximum in west central Sinai, Egypt. *Turk J Earth Sci* 24(5):475–493
- Faris M, Shabaan M, Shaker F (2017) Calcareous nannofossil bioevents at the Palaeocene/Eocene boundary in the Kharga

- Oasis, Western Desert of Egypt. *J Croat Geol Surv Croat Geol Soc*:179–199
- Faris M, Obaidalla NA, Metwally AA, Salman AM, Zaky AS (2018) Late Cretaceous–early Paleogene tectonic events at Farafra–Abu Minqar Stretch, Western Desert, Egypt: results from calcareous plankton. *Arab J Geosci* 11, Article number: 429
- Firth JV, Wise Jr, SW (1992) A preliminary study of the evolution of Chiasmolithus in the Middle Eocene to Oligocene of Sites 647 and 748, ODP Leg 120. *Proceedings of the Ocean Drilling Program Scientific Results*, volume 120, pp. 493–508. College Station, TX: Ocean Drilling Program
- Fisher CG, Hay WW (1999) Calcareous nannofossils as indicators of mid-Cretaceous paleofertility along an ocean front, US Western Interior. *Geological Society of America, Special Paper*, 332, pp 161–180
- Frieling J, Reichert GJ, Middelburg JJ, Röhl U, Thomas Westerhold T, Bohaty SM, Sluijs A (2018) Tropical Atlantic climate and ecosystem regime shifts during the Paleocene–Eocene Thermal Maximum. *Clim Past* 14:39–55
- Fuqua L, Bralower T, Arthur M, Patzkowsky M (2008) Evolution of calcareous nannoplankton and recovery of marine food webs after the Cretaceous–Paleocene mass extinction. *Palaios* 23:185–194
- Gibbs SJ, Bown PR, Bralower TJ (2006a) Ocean acidification and calcareous nannoplankton at the Paleocene–Eocene Thermal Maximum. F. Caballero (Ed.) et al., *Climate and biota of the early Paleogene*, p. 51. Abstract, Bilbao
- Gibbs SJ, Bown PR, Sessa JA, Bralower TJ, Wilson PA (2006b) Nannoplankton extinction and origination across the Paleocene–Eocene Thermal Maximum. *Science* 314:1770–1773
- Gingerich PD (2003) Mammalian response to climate change at the Paleocene/Eocene boundary: Polecat Bench record in the northern Big horn Basin, Wyoming. In: Wing SL, et al. (Ed.), *Causes and consequences of globally warm climates in the early Paleogene*. Geological Society of America, Special Paper 369, pp. 463–478
- Haq BU, Lohmann GP (1976) Early Cenozoic calcareous nannoplankton biogeography of the Atlantic Ocean. *Mar Micropaleontol* 1:119–194
- Hay WW (1964) The use of the electron microscope in the study of fossils. *Smithsonian Institution Annual Reports*, 1963: 409–415
- Hay WW, Mohler HP (1967) Calcareous nannoplankton from early Tertiary rocks at Pont Labau, France, and Paleocene–early Eocene correlations. *J Paleontol* 41(6):1505–1541
- Kahn A, Aubry MP (2004) Provincialism associated with the Paleocene/Eocene Thermal Maximum: temporal constraint. *Mar Micropaleontol* 52:117–132
- Kasem AM, Wise S, Faris M, Farouk S, Zahran E (2017) Calcareous nannofossil biostratigraphy of the Paleocene at the Misheiti section, East Central Sinai, Egypt. *Arabian Journal of Geosciences*, 10(20), pp.1–13.
- Kasem AM, Jr W, Faris M, Farouk S, Zahran E (2020a) Upper Paleocene-lower Eocene calcareous nannofossil stratigraphy at the Misheiti section, Central Sinai, Egypt. *Turk J Earth Sci* 29:242–256
- Kasem AM, Jr W, Faris M, Farouk S, Zahran E (2020b) Calcareous nannofossil stratigraphy across the Paleocene/Eocene transition at the Gunnah section, Farafra Oasis, Western Desert, Egypt. *J Geol* 128:371–387
- Khalil H, Al Sawy S (2014) Integrated biostratigraphy, stage boundaries and Paleoclimatology of the upper Cretaceous–lower Eocene successions in Kharga and Dakhala Oases, Western Desert, Egypt. *J Afr Earth Sci* 96(2014):220–242
- Khozyem H, Adatte T, Spangenberg JE, Tantawy A, Keller G (2013) Paleoenvironmental and climatic changes during the Paleocene–Eocene Thermal Maximum (PETM) at the Wadi Nukhul Section, Sinai, Egypt. *J Geol Soc Lond* 170:341–352
- Khozyem H, Adatte T, Spangenberg JE, Keller G, Tantawy AA, Ulianov A (2015) New geochemical constraints on the Paleocene–Eocene Thermal Maximum: Dababiya GSSP, Egypt. *Palaeogeogr Palaeoclimatol Palaeoecol* 429:117–135
- Martini E (1971) Standard Tertiary and Quaternary calcareous nannoplankton zonation. In: Farinacci A (editor), *Proceedings of the 2nd Planktonic Conference*, Roma, Italy, pp. 739–785
- Marzouk AM, Scheibner C (2003) Calcareous nannoplankton biostratigraphy and paleoenvironment of the late Cretaceous–Paleogene of the Galala Mountains, Eastern Desert, Egypt. *Courier Forschungsinsitut Senckenberg* 244:11–35
- Metwally AA, Mahfouz KH (2018) The Paleocene/Eocene (P/E) boundary along the eastern plateau of Kharga-Baris oases, Western Desert, Egypt. *J Afr Earth Sci* 147:569–584
- Monechi S, Angori E, Speijer RP (2000) Upper Paleocene biostratigraphy in the Mediterranean region: zonal markers, diachronism, and preservational problems. In: Andreasson FP, Schmitz B, Thompson EI, editors. *Early Paleogene Warm Climates and Biosphere Dynamics*, GFF, 122: 108–110
- Monechi S, Reale V, Bernaola G, Balestra B (2013) The Danian/Selandian boundary at Site 1262 (South Atlantic) and in the Tethyan region: biomagnetostratigraphy, evolutionary trends in fasciculoliths and environmental effects of the Latest Danian Event. *Mar Micropaleontol* 98:28–40
- Mutterlose J, Linnert C, Norris R (2007) Calcareous nannofossils from the Paleocene–Eocene Thermal Maximum of the equatorial Atlantic (ODP Site 1260B): evidence for tropical warming. *Mar Micropaleontol* 65:13–31
- Obaidalla, N A, Abdel-Maksoud N A, Hosny, A. H. and Mahfouz, K H (2017): Nature of the Paleocene/Eocene (P/E) boundary in Sinai, Egypt, *Journal of African Earth Sciences (Special Issue, Phanerozoic of Egypt)*, 136:44–60.
- Okada H, Bukry D (1980) Supplementary modification and introduction of code numbers to the low-latitude coccolith biostratigraphic zonation (Bukry, 1973; 1975). *Mar Micropaleontol* 5:321–325
- Ouda K, Berggren W, Abdel Sabour A (2013) Planktonic foraminiferal biostratigraphy of the Paleocene/Eocene boundary interval in the Dababiya Quarry Corehole, Dababiya, Upper Nile Valley, Egypt. *Stratigraphy* 9:213–227
- Ouda KH, Abdel BWA, Sabour A (2016a) Biostratigraphy of the Upper Palaeocene lower Eocene succession of Gebel El Aguz, north-eastern Kharga Oasis, Western Desert, Egypt. *Revue de Paléobiologie, Genève* 3(1):341–371
- Ouda KH, Berggren WA, Abdel Sabour A (2016b) Upper Palaeocene-lower Eocene biostratigraphy of Darb Gaga, Southeastern Kharga Oasis Western Desert, Egypt. *J Afr Earth Sci* 118:12–23
- Perch-Nielsen K (1971) Elektronenmikroskopische untersuchungen an Coccolithen und verwandten Formen aus dem Eozan von Danemark. *Biologiske Skrifter. Kongelige Danske Videnskaberne Selskab* 18(3):1–76
- Perch-Nielsen K (1985) Mesozoic calcareous nannofossils. In: Bolli, Saunders, Perch-Nielsen (eds) *Plankton stratigraphy*. Cambridge University Press, Cambridge, pp 329–426
- Pospichal JJ (1991) Calcareous Nannofossils across the K/T Boundary, ODP Leg 121, Site 752, Broken Ridge, In: Peirce, J., Weissel, J., et al., *Proc. ODP, Sci. Results*, 121: College Station, TX (Ocean Drilling Program), pp. 395–413
- Pospichal J, Wise SW Jr (1990) Paleocene to middle Eocene calcareous nannofossils of ODP Sites 689 and 690, Maud Rise, Weddell Sea, in: P.R. Barker, J.P. Kennett (Eds.) et al., *ODP, Sci. Results*, vol. 113 Ocean Drilling Program, College Station, TX, p. 613–638

- Raffi I, De Bernaola B (2008) Response of calcareous nannofossils to the Paleocene–Eocene Thermal Maximum: observations on composition, preservation and calcification in sediments from ODP Site 1263 (Walvis Ridge, SW Atlantic). *Mar Micropaleontol* 69:119–138
- Raffi I, Backman J, Pälike H (2005) Changes in calcareous nannofossil assemblage across the Paleocene/Eocene transition from the paleo-equatorial Pacific Ocean. *Palaeogeogr Palaeoclimatol Palaeoecol* 226:93–126
- Raffi I, Backman J, Zachos JC, Sluijs A (2009) The response of calcareous nannofossil assemblages to the Paleocene Eocene Thermal Maximum at the Walvis Ridge in the South Atlantic. *Mar Micropaleontol* 70:201–212
- Romein AJT (1979) Lineages in early Paleocene nannoplankton. *Utrecht Micropaleontol Bull* 22:18–22
- Roth PH (1986) Mesozoic palaeoceanography of the North Atlantic and Tethys Oceans. In: Summerhayes, CP Shackleton, N.J. (Eds.), *North Atlantic Palaeoceanography*. Geological Society of London, Special Publication, V. 21, pp. 299–320
- Roth PH, Krumbach KR (1986) Middle Cretaceous nannofossil biogeography and preservation in the Atlantic and Indian Oceans: implications for palaeoceanography. *Mar Micropaleontol* 10:235–266
- Said R (1960) Planktonic foraminifera from the Thebes Formation, Luxor, Egypt. *Micropaleontology* 6:277–286
- Self-Trail J, Powars D, Watkins D, Wandless G (2012) Calcareous nannofossil assemblage changes across the Paleocene–Eocene Thermal Maximum: evidence from a shelf setting. *Mar Micropaleontol* 92:61–80
- Stradner H (1969) The nannofossils of the Eocene Flysch in the Hagenbach Valley (Northern Vienna Woods) Austria. *Rocz Pol Towarz Geol* 39:403–432
- Tantawy A (1998) Stratigraphical and paleoecological studies on some Paleocene–Eocene successions in Egypt. Unpub. Ph.D. Thesis, Aswan Fac. Sci., South Valley Univ., Egypt, 273 pp
- Tantawy AA (2003) Calcareous nannofossil biostratigraphy and paleoecology of the Cretaceous Tertiary transition in the central eastern desert of Egypt. *Mar Micropaleontol* 47:323–356
- Tantawy AA (2006) Calcareous nannofossil of the Paleocene–Eocene transition at Qene Region, Central Nile Valley, Egypt. *Micropaleontology* 52(3):193–222
- Tantawy AA (2011) Calcareous nannofossils across the Cretaceous–Tertiary boundary at Brazos, Texas, U.S.A.: extinction and survivorship, biostratigraphy, and paleoecology. In G. Keller and T. Adatte, eds., *The end-Cretaceous mass extinction and the Chicxulub impact in Texas*, Society of Economic Mineralogists and Paleontologists Special Publication 100, Tulsa, Oklahoma, PP. 157–178
- Thibault N, Gardin S (2007) The late Maastrichtian nannofossil record of climate change in the South Atlantic DSDP Hole 525A. *Mar Micropaleontol* 65:163–184
- Thierstein HR (1981) Late Cretaceous nannoplankton and the change at the Cretaceous–Tertiary boundary. In: Warme JE, Douglas RG, Winterer EL (eds) *The Deep Sea Drilling Project: a decade of progress*. Special Publications of SEPM, vol 32. The Society of Economic Paleontologists and Mineralogists, Tulsa, pp 355–394
- Tremolada F, Bralower TJ (2004) Nannofossil assemblage fluctuations during the Paleocene–Eocene Thermal Maximum at sites 213 (Indian Ocean) and 401 (North Atlantic Ocean): palaeoceanographic implications. *Mar Micropaleontol* 52:107–116
- Varol O (1989) Palaeocene calcareous nannofossil biostratigraphy. In: Crux JA, Van Heck SE (editors), *Nannofossils and their applications*. British Micropaleontological Society, 12, pp. 267–310
- Von Salis K, Monechi S, Bybell LM, Self-Trail J, Young JR (2000) Remarks on the calcareous nannofossil genera *Rhomboaster* and *Tribrachiatulus* around the Paleocene/Eocene boundary. *Early Paleogene Warm Clim Biosphere Dyn GFF* 122:138–140
- Watkins DK (1989) Nannoplankton productivity fluctuations and rhythmically-bedded pelagic carbonates of the Greenhorn Limestone (upper Cretaceous). *Palaeogeogr Palaeoclimatol Palaeoecol* 74:75–86
- Wei W, Wise SW Jr (1990) Biogeographic gradients of middle Eocene–Oligocene calcareous nannoplankton in the South Atlantic Ocean. *Palaeogeogr Palaeoclimatol Palaeoecol* 79:29–61
- Westerhold T, Röhl U, McCarren HK, Zachos JC (2009) Latest on the absolute age of the Paleocene–Eocene Thermal Maximum (PETM): new insights from exact stratigraphic position of key ash layers + 19 and – 17. *Earth Planet Sci Lett* 287:412–419
- Williams JR, Bralower TJ (1995) Nannofossil assemblages, fine-fraction stable isotopes, and the paleoceanography of the Valanginian–Barremian (Early Cretaceous) North Sea Basin. *Paleoceanography* 10:815–839
- Youssef MA (2015) Evaluation of foraminifera and calcareous nannofossils changes across the late Paleocene/early Eocene transition at Nag El-Quda section, Upper Nile Valley, Egypt. *Geosci J* 19:641–654
- Youssef M (2016) Calcareous nannofossils and paleoenvironments of the Palaeocene/Eocene Thermal Maximum (PETM) interval in central Egypt. *J Afr Earth Sci* 114:203–219
- Zachos JC, Röhl U, Schellenberg SA, Sluijs A, Hodell DA, Kelly DC, Thomas E, Nicolo M, Raffi I, Lourens LJ, McCarren H, Kroon D (2005) Rapid acidification of the ocean during the Paleocene–Eocene Thermal Maximum. *Science* 308:1611–1615